ELECTROSTATIC GENERATION WHILE TANK WASHING AND IGNITION HAZARDS OF FUEL AIR MIXTURES

by

George Economou

B.S. in Naval Architecture and Marine Engineering
Massachusetts Institute of Technology
June 1975

SUBMITTED IN PARTIAL FULFILLMENT

OF THE REQUIREMENTS FOR THE

DEGREE OF MASTER OF SCIENCE

IN NAVAL ARCHITECTURE AND MARINE ENGINEERING

at the

MASSACHUSETTS INSTITUTE OF TECHNOLOGY

September 1975
(i.e. February 1976)

Signature redacted

Signature of Author .....
Department of Ocean Engineering
(September 1975)

Signature redacted

Certified by .....
Thesis Supervisor

Signature redacted

Certified by ...
Departmental Reader

Signature redacted

Accepted by ....
Chairman, Departmental Committee on Graduate Students

ELECTROSTATIC GENERATION WHILE TANK WASHING AND IGNITION HAZARDS OF FUEL AIR MIXTURES

by

George Economou

Submitted to the Department of Ocean Engineering September, 1975, in partial fulfillment of the requirements for the degree of Master of Science in Naval Architecture and Marine Engineering.

ABSTRACT

The causes of explosions occurring in tankers during tank washing operations are yet unknown. Tests, conducted with simulated tank washing using water pressures of less than 20 psi and flows of up to 1600 cc/sec inside a tank of cubical dimension 1.36m showed that substantial electrification could develop. Maximum fields up to 2200 V/m were measured and varied with changing water flows. The ignition of fuel vapor, air, and water mixtures by electrical discharges was studied in a small pressure vessel. When sufficient energy was discharged a spark breakdown was found to ignite an explosion, if the fuel air composition lay inside the explosive range. An isolated statically charged object or an ungrounded person was found to carry enough charge to initiate an explosion. On the other hand, corona discharges of up to several hundred microamps were not incendiary.

Thesis advisor: Chatham M. Cooke

Title: Assistant Professor of Electrical Engineering

ACKNOWLEDGEMENTS

I would like to express my sincere appreciation to Professor Chathan M. Cooke for his daily guidance and assistance through all phases of this project and to Professor A. Douglas Carmichael for suggesting the problem.

To Joan Dowd I wish to express my deepest thanks for her help and encouragement throughout this endeavor.

TABLE OF CONTENTS

CHAPTER I

INTRODUCTION

For many years the world tanker industry has had an excellent safety record. However, the three VLCC explosions which occurred in December 1969 gave rise to great concern and as a result many studies were carried out in an effort to explain the cause of these disasters. Many concluded that if there was a common cause to the three explosions, then static electricity appears to be the most probable one.[1,2,3]

It was considered that the mist produced by breaking up of the water jets used for cleaning would carry electrostatic charges. This distribution of charge in the tank could create an electrostatic field and, if of sufficient magnitude, electrical breakdown might occur thus leading to an explosion.[4,5,6]

In order to gain an understanding of the creation of the electrostatic field and the subsequent breakdown, which could initiate an explosion, two experiments were conducted. In the first, an effort was made to create an atmosphere similar to that when tank washing. For this reason tap water was sprayed against a plate hanging inside a model tank and the mechanisms of charge generation and decay were studied. The second experiment had to do with explosions of fuel-air-water mixtures carried out in a small test bomb. Because of the nature of the problem we concluded that high voltage ignition data would be directly pertinent to ignition by static discharges. The method of igniting gases with discharge arcs from capacitors charged to high voltage was employed and results and conclusions are presented in subsequent chapters.

CHAPTER II

ELECTRIFICATION PRODUCED BY RUPTURE OF WATER DROPS

It has been observed that when water drops break up electrical charges are separated. This phenomenon was first investigated by Lenard who measured charge generation at the base of a waterfall.[7,8] After further measurements with laboratory experiments, he postulated that this observation was associated with the splashing of water rather than the mere flow of water through air.[9] He was thus able to show that strong electrification developed when water drops hit an obstacle.

When water hits a solid surface a liquid "crown" is thrown up. As this crown expands, jets develop from its upper periphery, which subsequently break up into liquid fragments. It has been observed that the number of liquid fragments is proportional to both the size of the water drops as well as the impact velocity.[10] The fragments of the broken drops communicate a net positive charge to the surface, thus carrying an excess of negative charge to the surrounding atmosphere. Many investigators have tried to measure the charge generated by splashing. As an order of magnitude approximation 3.34 to 33.4 x 10^{-4} coul/m^3 seems to be a representative number for velocities of about 15m/sec and drop sizes of a few millimeters in diameter.

The size of the charge measured at the surface where the water impinges, depends on the salinity of the water. When drops consisting of pure water or dilute salt solutions are splashed on a surface, a net positive charge is communicated to it and hence negative charge to the atmosphere. As the concentration of salt in the water increases

the amount of charge communicated to the surface becomes less and after a certain point, the sign of the charge is reversed. This reversal in sign occurs for solutions ranging betweem 0.006% and 0.01% by weight of salt.[8,11]

The object of the experiment was to study the mechanisms of charge generation and decay created by the washing procedure in a tank. By directing a spray from a washing nozzle into the tank, it was intended to determine the magnitude and polarity of any charge and the associated electric field produced by its use.

The effect on the field of changing different parameters was also investigated. These changes include:

1. Varying water pressure and hence flow and velocity of the water jet;
2. Changing the position of the spraying nozzle;
3. Introducing grounded objects in the tank;
4. Ventilating the tank;
5. Spraying the water against different surface coatings used by the industry in coating tanks carrying petroleum products.

CHAPTER III

A. Experimental Apparatus

So as to study the phenomena associated with charge generation from a spraying water jet, a model tank was constructed. The model tank design was arranged so to enable the study of the variation in electrostatic field with changes in water flow, ventilation, and different surface coatings. Grounded objects placed in the tank were used to examine whether "free" equipment could alter the character of the field. The various equipment constituting the experimental apparatus are described in detail below.

Tank

An aluminum tank of overall dimensions 1.4m x 1.2m x 1.5m was constructed from 0.20 cm thick sheet. So as to be able to observe various phenomena occurring during washing operations, one side of the tank was plexiglas sheet. Hanging inside the tank was a 0.9m x 1.2m plate positioned at a distance of 1.1m from the spraying nozzle. The plate was insulated and separately grounded from the rest of the tank and could be replaced easily. In this way the effects of different materials on charge generation and decay could be studied.

So as to decelerate corrosion of the tanks some corrosion resistant surface coatings have been developed. Field generation and decay was investigated with four different such coatings. Two of the materials were inorganic zinc silicate coatings (Dimetcoat 3 and 4), while the two others were epoxies (Amercoat 81/82 and a high solids

amine cured epoxy, Amercoat 395).

Nozzle

Mounted on one side of the tank was a spraying nozzle, supplied by tap water. It was made from brass pipe 3.81 cm O.D. and 3.18 cm I.D., closed at the spraying end where seventeen 0.16 cm diameter holes had been drilled. The nozzle could be also placed near a corner at the top plate of the tank so that the water jet was directed downwards. When desired the nozzle could be also grounded, so as to observe any contribution of the water flowing through it to the total charge accumulated in the model tank.

Fan

In order to investigate the effect of ventilation on the buildup and decay of the electrostatic field a "mini boxer" fan of 46 CFM with overall blade diameter 8.26 cm, was mounted at the center of one side of the tank. The fan could be also placed at a lower corner on the plexiglas sheet. The vent ports used for mounting the fan were openings on the tank of 8.9 cm diameter.

Generating Volt Meter (GVM)

The field buildup and decay were measured through a GVM with 8 segments, having an overall diameter 8.26 cm and mounted in a hole of 8.9 cm diameter, of maximum sensitivity 5 V/m. So as to get field measurements corresponding to the maximum field present in the tank, the GVM was permanently positioned at the center of the top plate. The calibration curve used for converting the GVM measurements is shown in Figure 1.

Figure 2 is a sketch showing an outline of the tank with the various positions of the fan and the spraying nozzle, the GVM and the test sheet. A photograph of the tank while running water is also portrayed

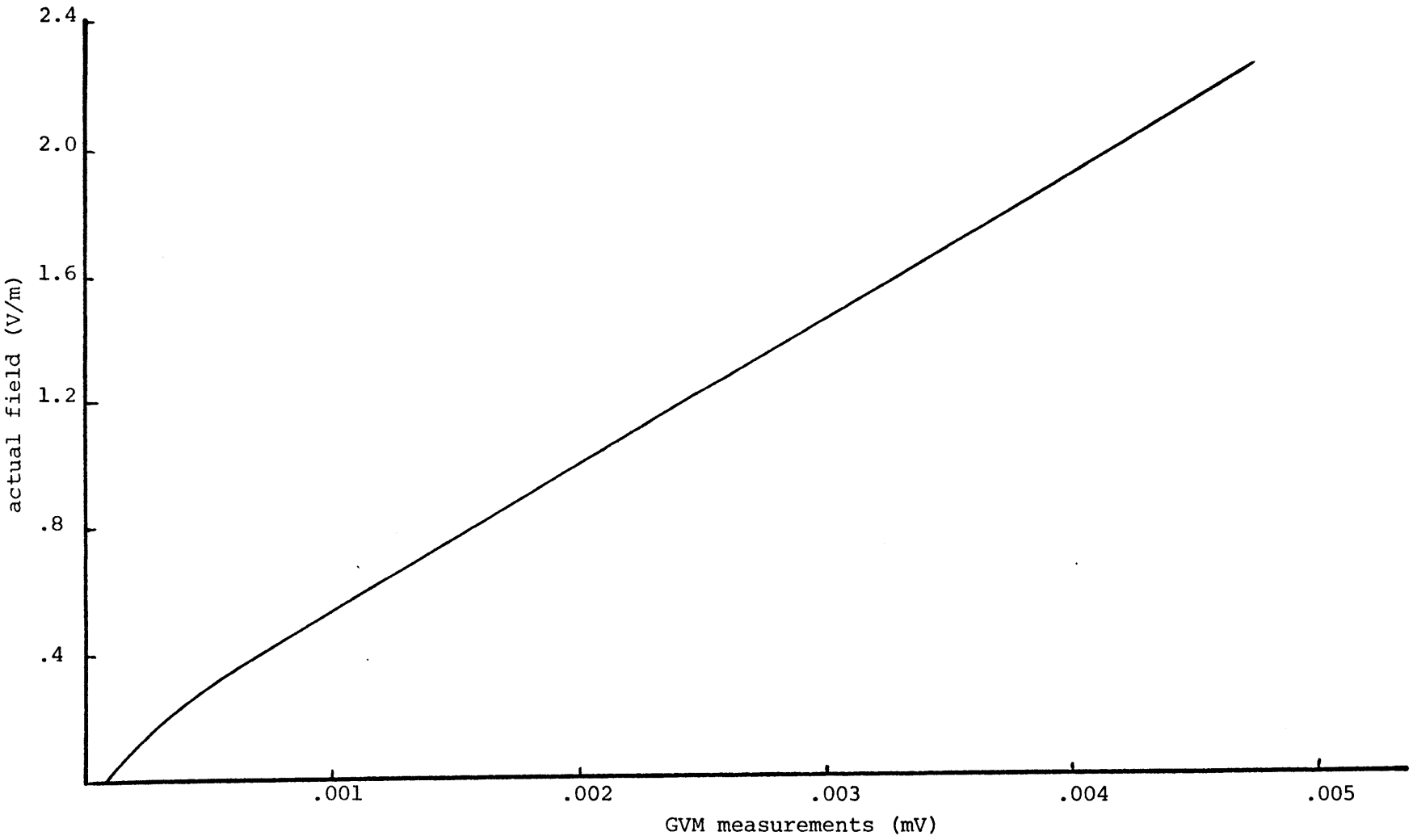

FIGURE 1: Calibration curve for the GVM

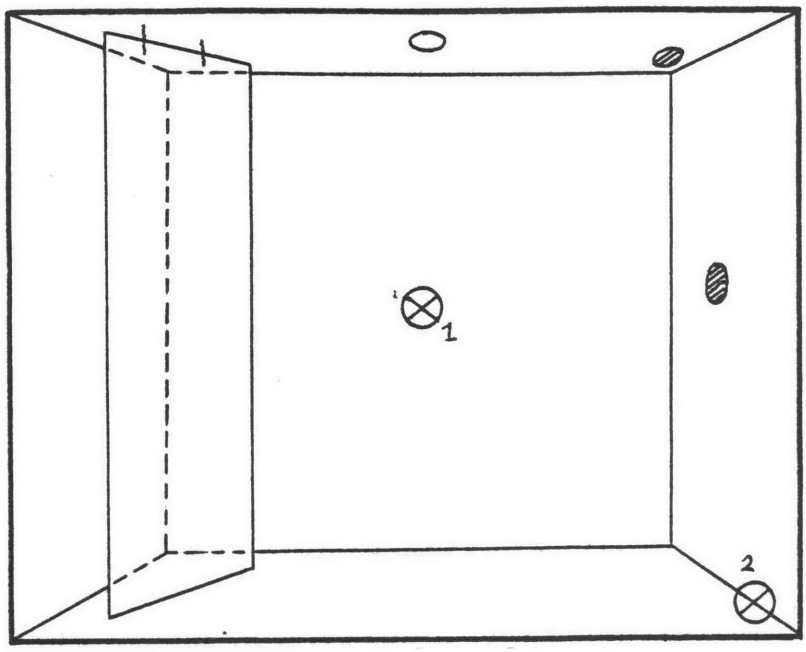

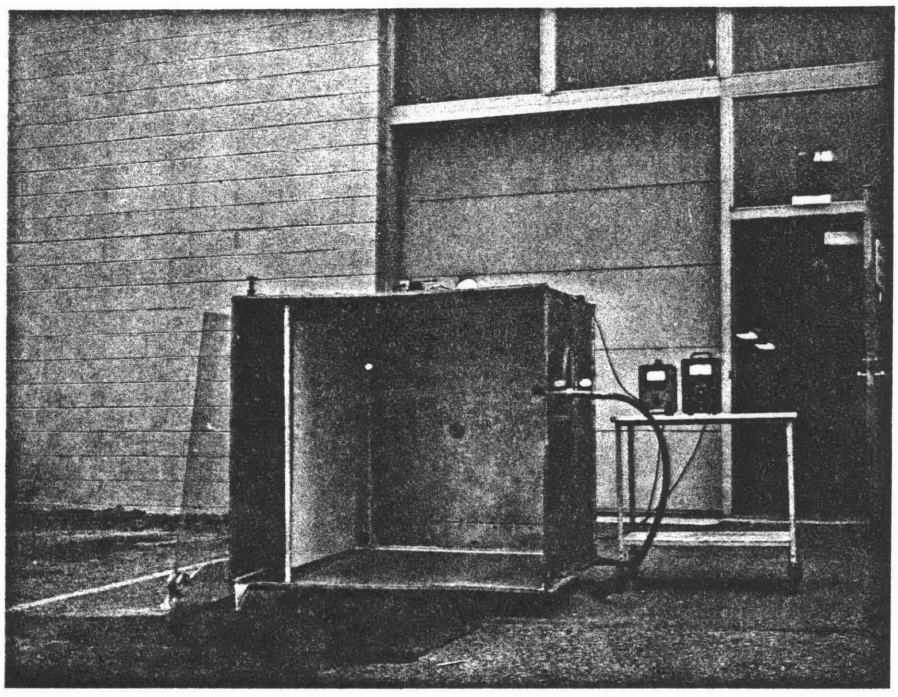

FIGURE 2: The model tank

⊗ fan positions; 1:at center of back side of tank
2:at lower corner on lucite sheet

nozzle positions perpendicular to side where openings exist

GVM permanently placed at center of top plate

B Experimental Procedure

The procedure for conducting the experiment was very simple. The flow of the water was regulated by controlling the pressure at the nozzle. A graph of pressure vs flow and velocity is shown in Figure 3. At the initial stages of charge generation field measurements were taken every 10 seconds. Subjsequently as the field growth slowed values were taken every minute and later every two minutes as equilibrium was approached. After equilibrium was reached the water was shut off and the charge was allowed to decay. Field measurements were taken at similar intervals, again every 10 secons initially and one and two minutes later on, until the charge decayed completely.

In order to determine whether the creation of the field was due to the jet of water splashing against the hanging plate, or to the water dripping from the plate to the bottom of the tank, measurements of field strengths were also conducted after the bottom of the tank had been completely covered with heavy cotton cloths. So as to see if the field was influenced by the detailed shape of the ship tank, which is more complicated than a mere rectangular box, various supported objects (spheres, rods) were introduced and measurements were conducted.

The effects of ventilation were studied using the same procedure for measuring field buildup and decay. For some measurements the fan was on both during field buildup and decay, while for others it was only turned on after the water was shut off.

Finally, some of the above described measurements were taken for different positions of the spraying nozzle. The results of such changes are described in the next chapter.

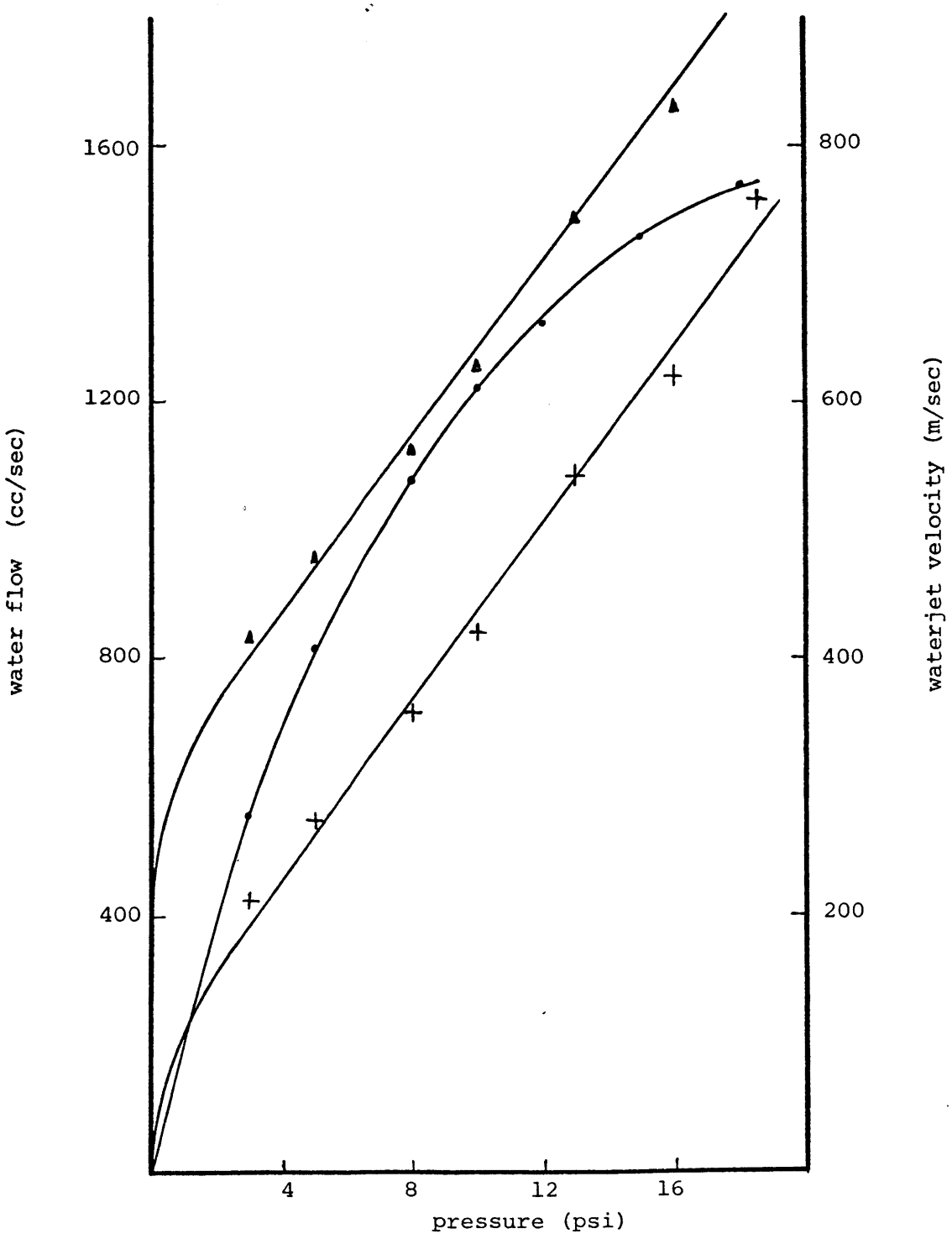

FIGURE 3: Water flow and water jet velocity versus pressure measured at the spraying nozzle
+ water jet velocity across
• water flow
▲ water jet velocity downwards

CHAPTER IV

A. Field Buildup and Decay

When the water is turned on, the field in the tank immediately begins to build up. It rises sharply at first and then slows down as it approaches its peak value after about a half hour's time. During the first stages of the field buildup the field is small and hence charge loss to the tank walls is presumably insignificant. For these initial stages the field growth follows an equation of the form $E=E_{max}(1-e^{-at})$. The value of the coefficient a varies only slightly with different flows and has a value of approximately 0.0028 sec^{-1} for pressures ranging between 5 and 18.7 psig. Subsequently at higher fields charge transfer to the walls of the tank becomes significant and limits the rate at which the field rises so that eventually a steady-state maximum is attained. At this equilibrium value the rate of charge generation due to splashing equals the rate of charge dissipation, which is a result of charged particles coming in contact with the walls of the tank. Figure 4 shows the field buildup vs. time for different flows.

As soon as the water is turned off there is a sudden upward jump of the field of about 30%. This phenomenon is associated with the fact that the water jet passes directly beneath the GVM as explained in a later part.

The decay of the field is also rapid at the beginning, slowing down eventually. However, it does not follow a simple exponential curve as indicated by other investigators.[11,12,14] Nevertheless, it is true that if the field decay is examined over a limited field range (a factor of 3 to 4 or less) an exponential curve of the form $E = Ae^{-at}$ can be applied.

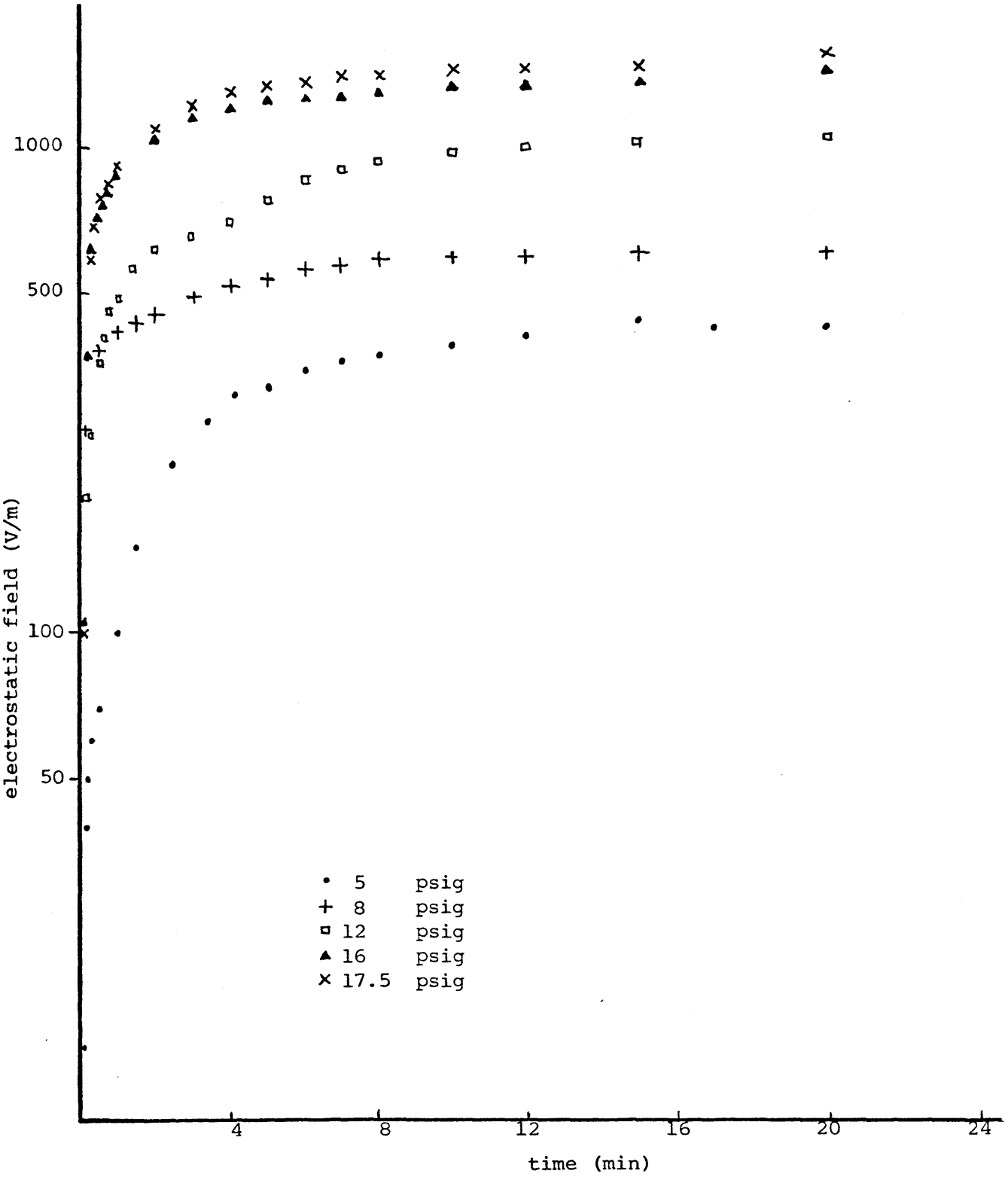

FIGURE 4: Field buildup for various flows when water jet was directed against the hanging plate

Regarding our experiments, whose field decays are portrayed in Figure 5, when the equation $E = E_{max} e^{-at}$ was applied to the initial stages of the decay the coefficient a was found to be approximately 0.01 regardless of water flow. As time goes by the decay rate decreases as seen by the smaller slope of the field-time curve. For this reason when the same equation, $E = E_{max} e^{-at}$, was applied towards the final stages the value of a was found to be smaller by a factor of about 10. In other words the decay time constant $\tau=1/a$ changed by as much as 10, being 100 sec. initially and as long as 1100 sec. for smaller fields.

It turned out that a also depended on the maximum field and hence there was not a unique a for each field value. This complex behavior may be associated with the dynamics of charge redistribution at shut off or due to non-linear diffusion to the tank walls.

The measurements taken while conducting the experiments show that they are both consistent and repeatable. However, there were variations in the charging and decay rates when different parameters were changed. The effects of these parameters are examined in the next part.

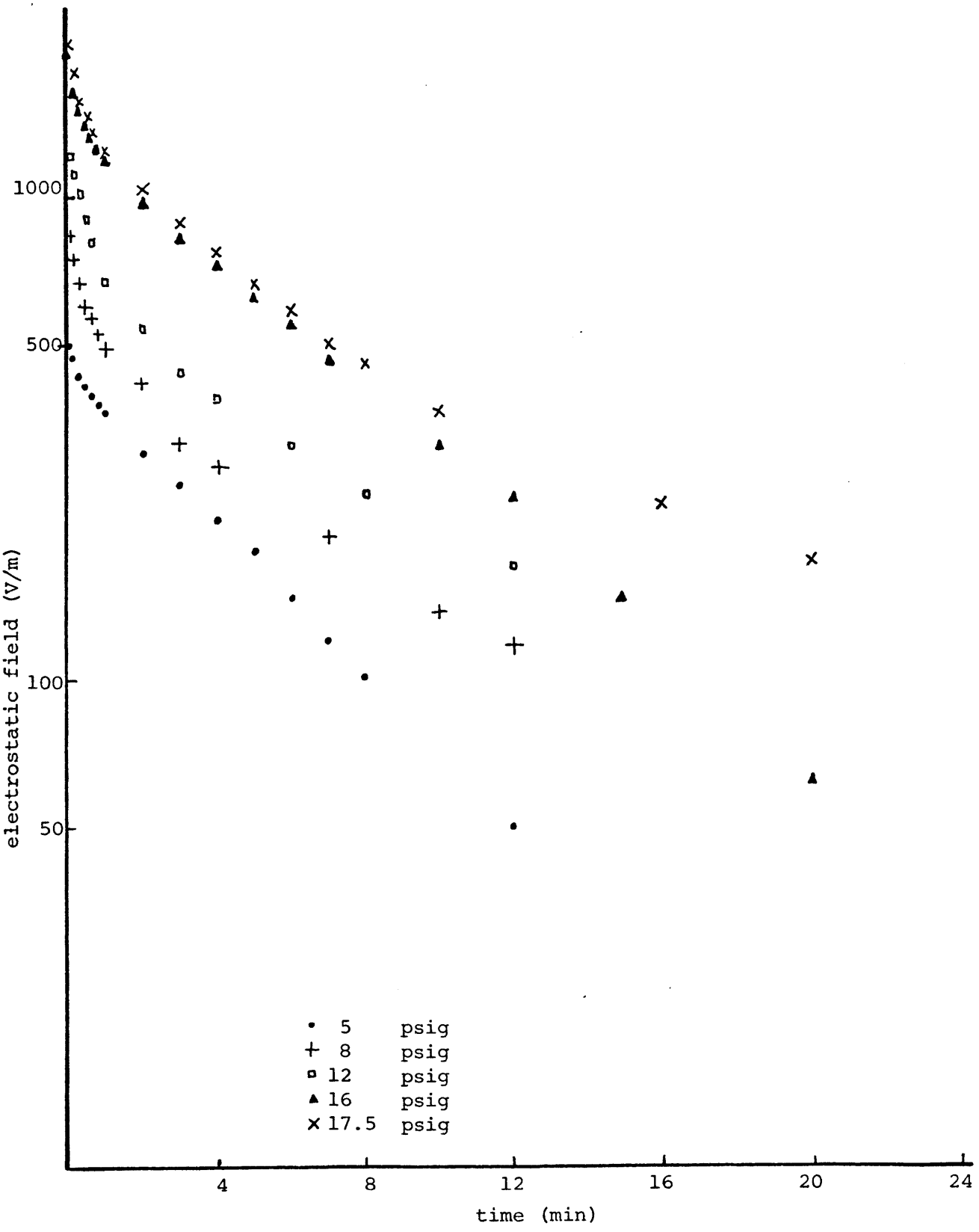

FIGURE 5: Field decay for various flow when water jet was directed against the hanging plate before shutoff

B. Water Flow

The initial design and positioning of the nozzle forced the water jet to pass directly underneath the GVM at a distance of 40 cm. We felt that this fact could alter the readings obtained by the GVM since the water jet was grounded by nature. This was proved correct when the water jet was diverted downwards while mounted near a corner at the top plate of the tank away from the GVM. For the same flow the measurements were higher than when the water jet was splashing against the plate. This is shown in Figures 6 and 7 which give both the charging and decay rates for various flows and may be compared with the values for the 5 psig flow of Figures 4 and 5. The main effect again was the production of a negative field in accordance with what was said earlier.

Figures 4, 5, 6, and 7 help us observe that the higher the flow rate the faster the rate at which the field increases and the bigger the value of the maximum field. The table constructed below shows the value of the maximum field for various flows.

Table 1

Water flow	5	5*	8	10*	12	16	17.5	18.7*
Maximum field	503	680	842	1377	1447	2005	2098	2237

The above mentioned Figures also show that the field rises to a value of 2/3 its peak value in the first minute or two and also decays to half its maximum value within the first two minutes.

*Marks flow when water jet was directed downwards.

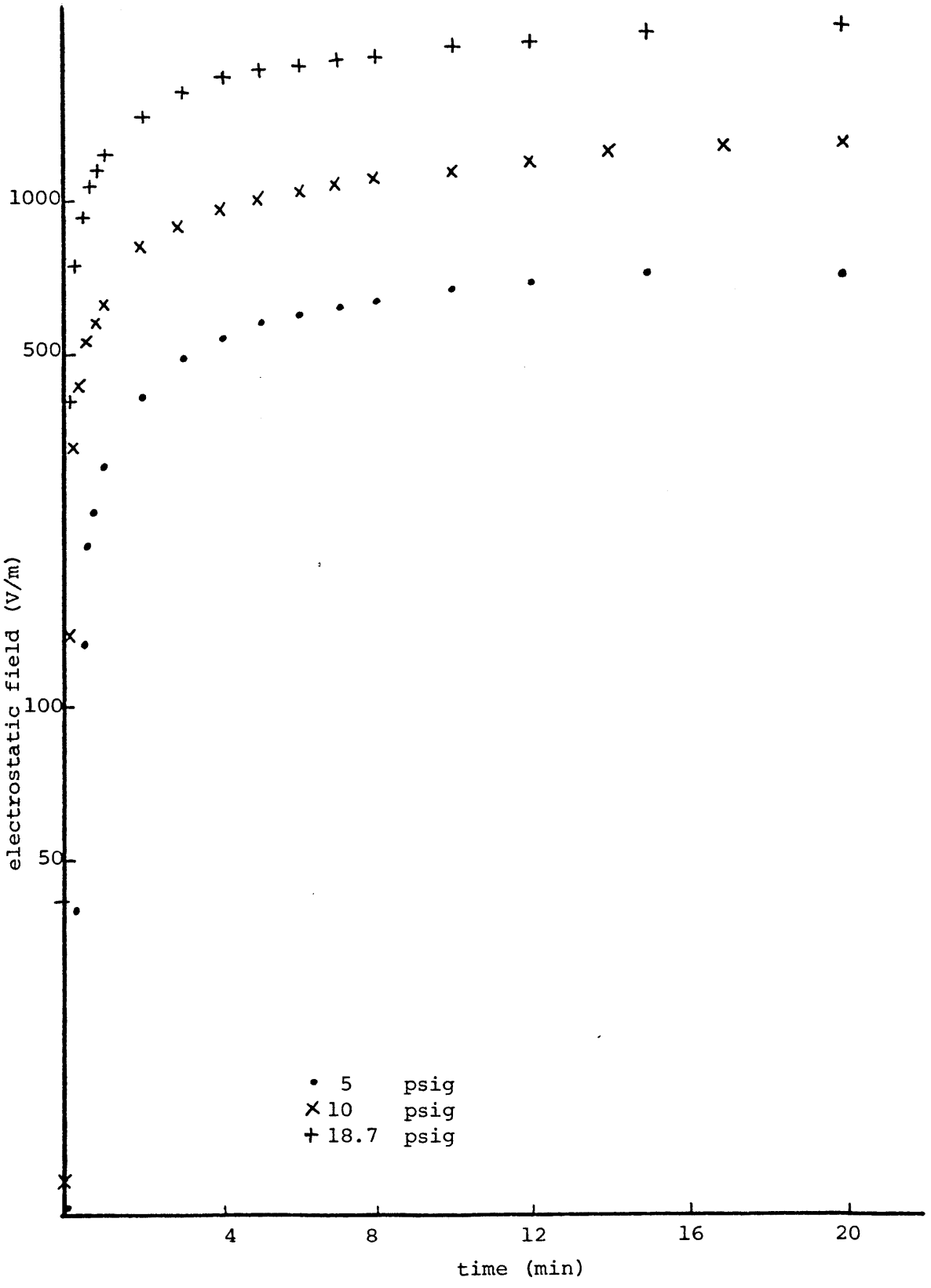

FIGURE 6: Field buildup when water jet was directed downwards

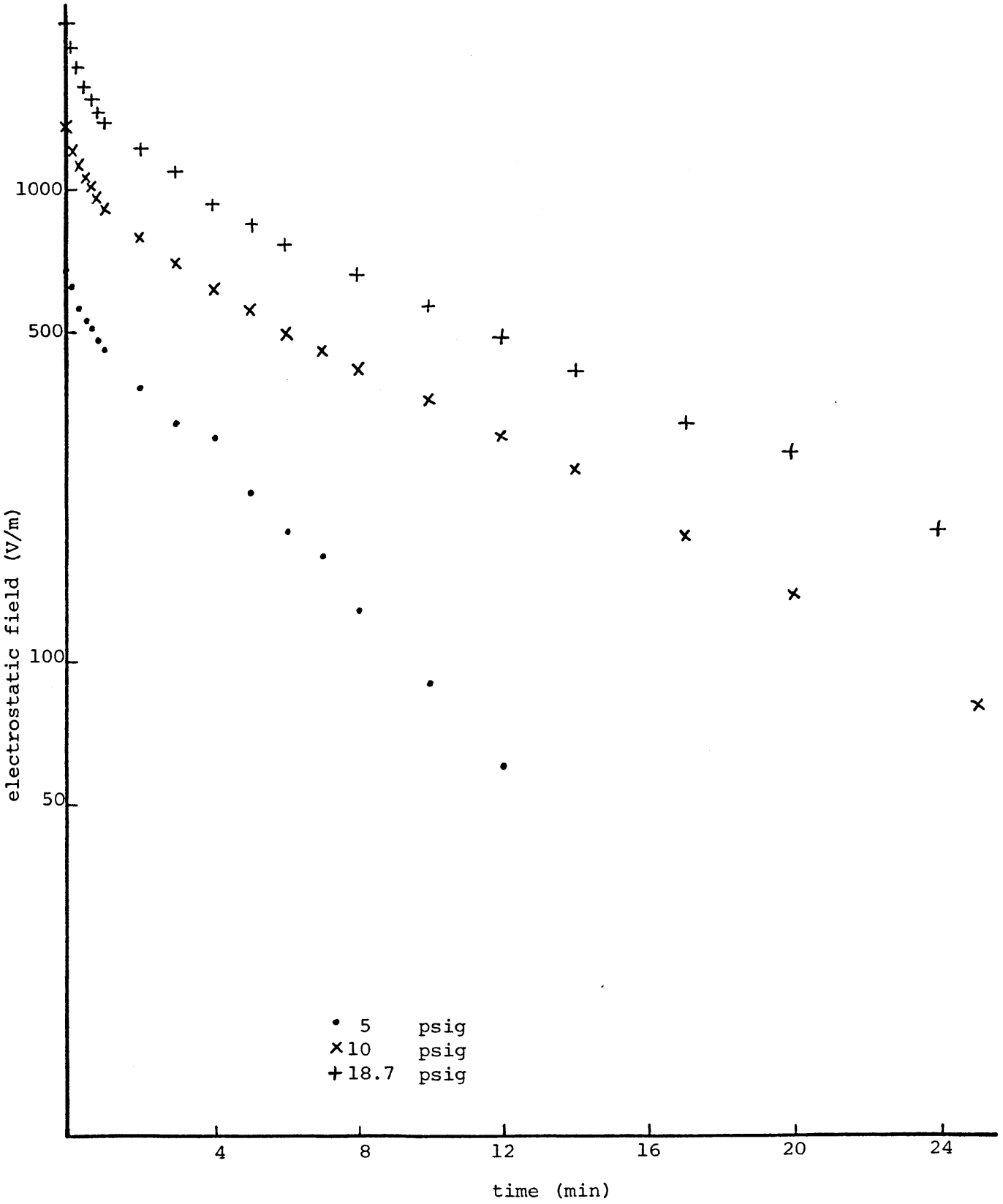

FIGURE 7:. Field decay when water jet was directed downward before shutoff

C. Suspended Objects

In order to examine the effect on the field of various equipment present in the tank while washing, grounded spheres or rods were introduced in our test tank. Both the spheres and the rods were placed halfway between the bottom and the top plates directly beneath the GVM. We felt that if there was going to be any change in the magnitude of the field the biggest effect would be achieved when positioning the objects as described above. Figures 8 and 9 show graphs of the charging and decay rates for flows with and without objects present. No substantial difference in the field was recorded.

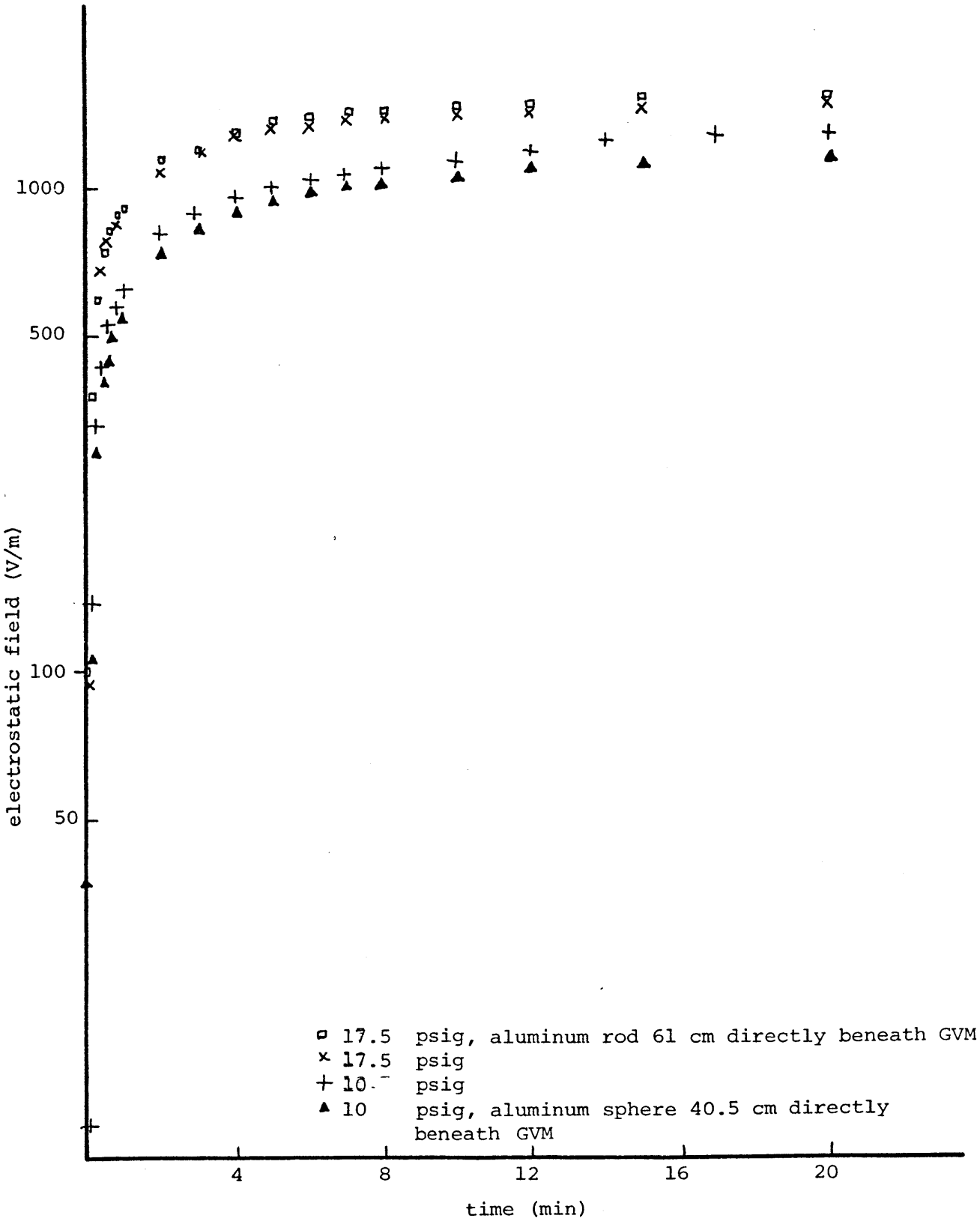

FIGURE 8: Field buildup when grounded supported objects were introduced in the tank

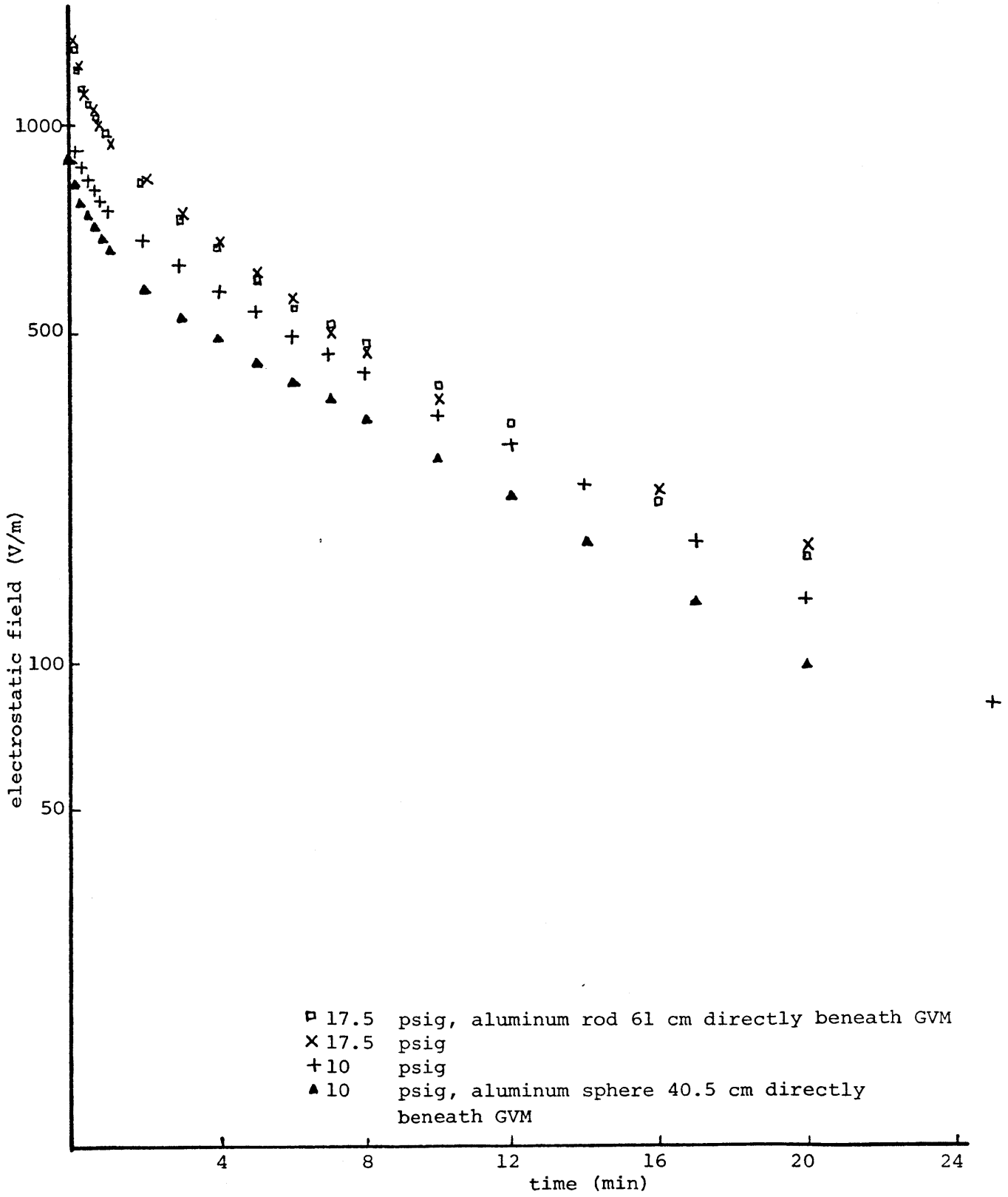

FIGURE 9: Field decay when grounded supported objects were introduced in the tank

D. Ventilation

Small holes present in the tank which had been purposely left uncovered showed the effect of air currents on the level of the electrostatic field. It was evident that whenever the wind blew, the field would drop momentarily. This was due to the transport of negative charge by the wind to the walls of the tank.

This phenomenon was more evident when the effect of ventilation of the tank was examined. For this purpose the small fan described earlier was mounted at the center of one side of the tank. Later the fan was placed at a lower corner (See Figure 2), and measurements were again taken. Figure 10 shows graphs of the field vs time for one of these positions of the fan and also measurements taken with the fan off. It can be clearly seen that when the fan was used both the charging rate and the value of the maximum field were lower.

It has been shown that the hydrocrabon vapor concentration in the tank at any time is a function of the initial concentration and the rate of ventilation and may be given by the expression

$$C = C_o e^{-kt}$$

where k is the ventilation rate divided by the tank volume. In this expression, the time for one equivalent volume turnover of the tank is thus equal to 1/k. Since for our model tank k = 0.517, the time for one equivalent turnover of the tank is estimated to be 1.93 min. When one substitutes the field for the hydrocarbon concentration, this relationship becomes

$$E = E_o e^{-kt}$$

where E_o is the initial field intensity. The validity of the equation

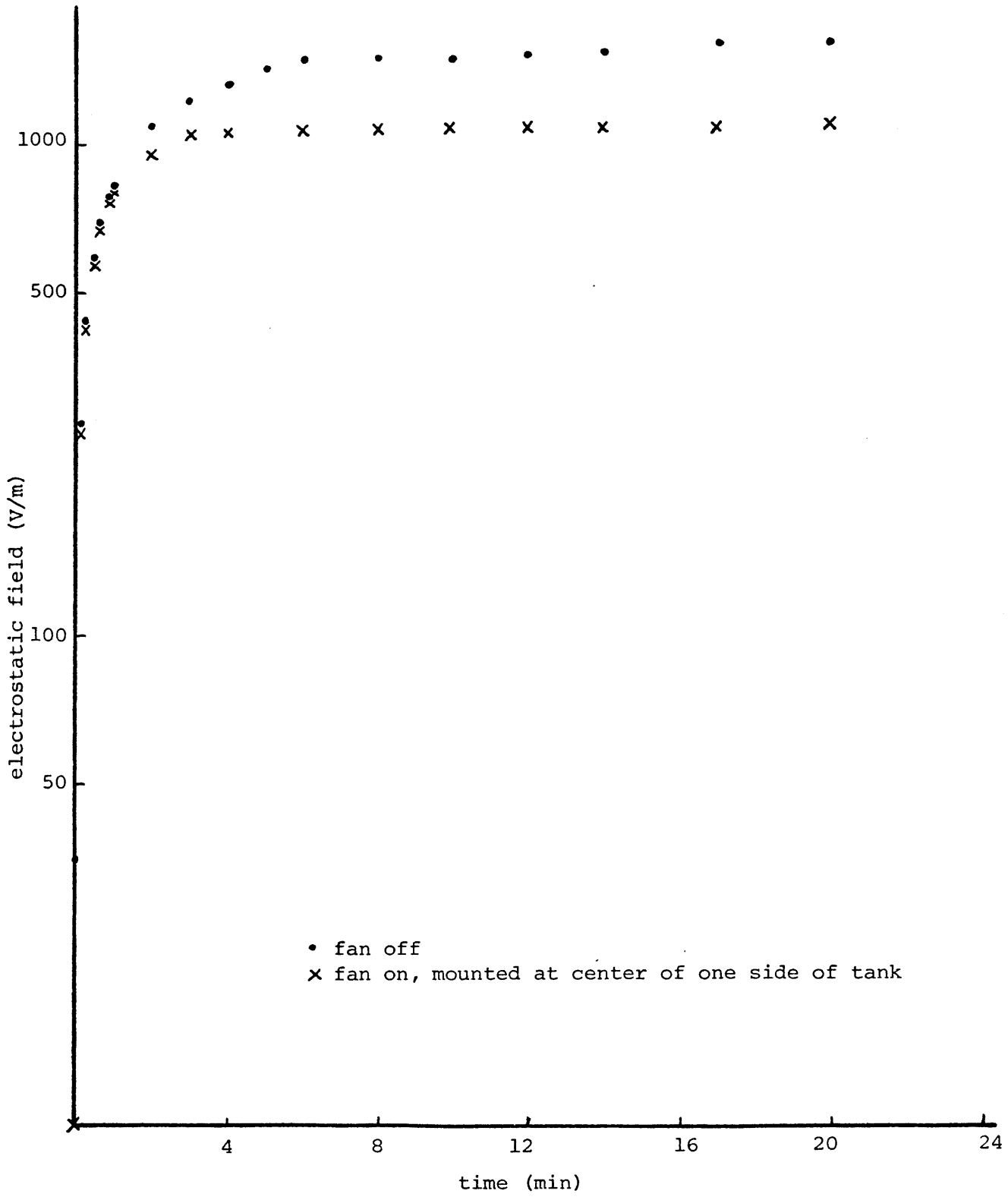

FIGURE 10: Field buildup for a pressure of 10 psig with and without the fan on

was checked by deriving theoretical values of the field from data taken when the fan was not used. These agree with actual values of the field measured when the fan was on and the field decaying.

Figure 11 shows the decaying field for a flow at 10 psig when the fan was both off and on and for various positions as well. It can be seen that the decay rate is accelerated by as much as 500% when compared with measurements taken without a fan.

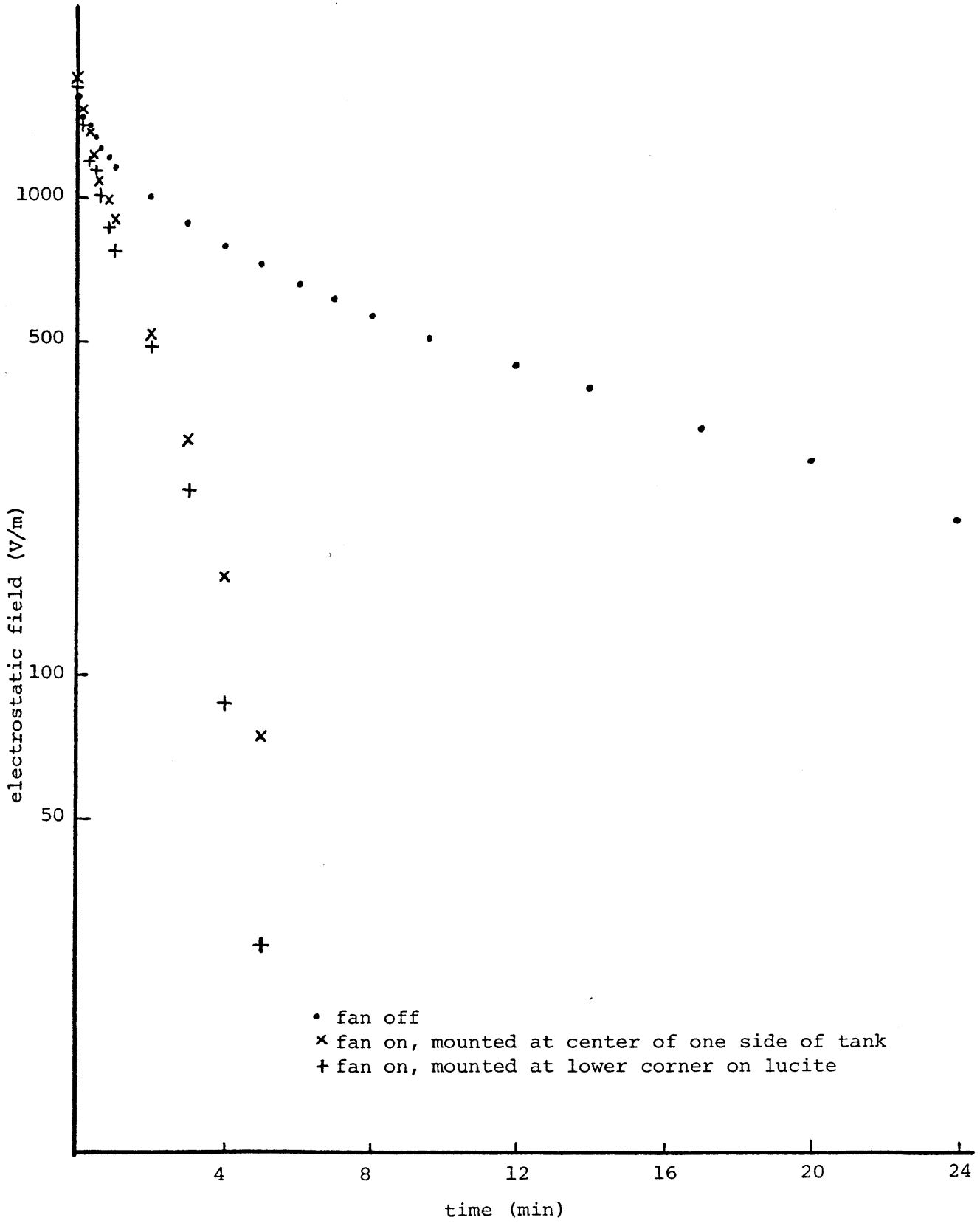

FIGURE 11: Field decay for a pressure of 10 psig before shutoff with and without the fan on, as well as for various positions of the fan

E. Material

The effect of the material of the plate against which the water splashes was also examined. As was explained earlier different coatings used in tanks which are filled with petroleum products were investigated. The effects on both the charging and the decay rates are shown in Figures 12 and 13. Tests when using the aluminum plate at the same flow are also portrayed for comparison. It can be seen that all coatings act in a way to increase the magnitude of the field. Even though the differences are not large, one observes that the inorganic materials give rise to a bigger field than organic materials by about 15%.

The overall decay times depend on the peak value of the field present in the tank and not on the material used to coat the hanging plate. Since the coated area was less than 1/6 the overall surface area, perhaps these coating materials would affect the decay rates as well if the tanks had been completely coated.

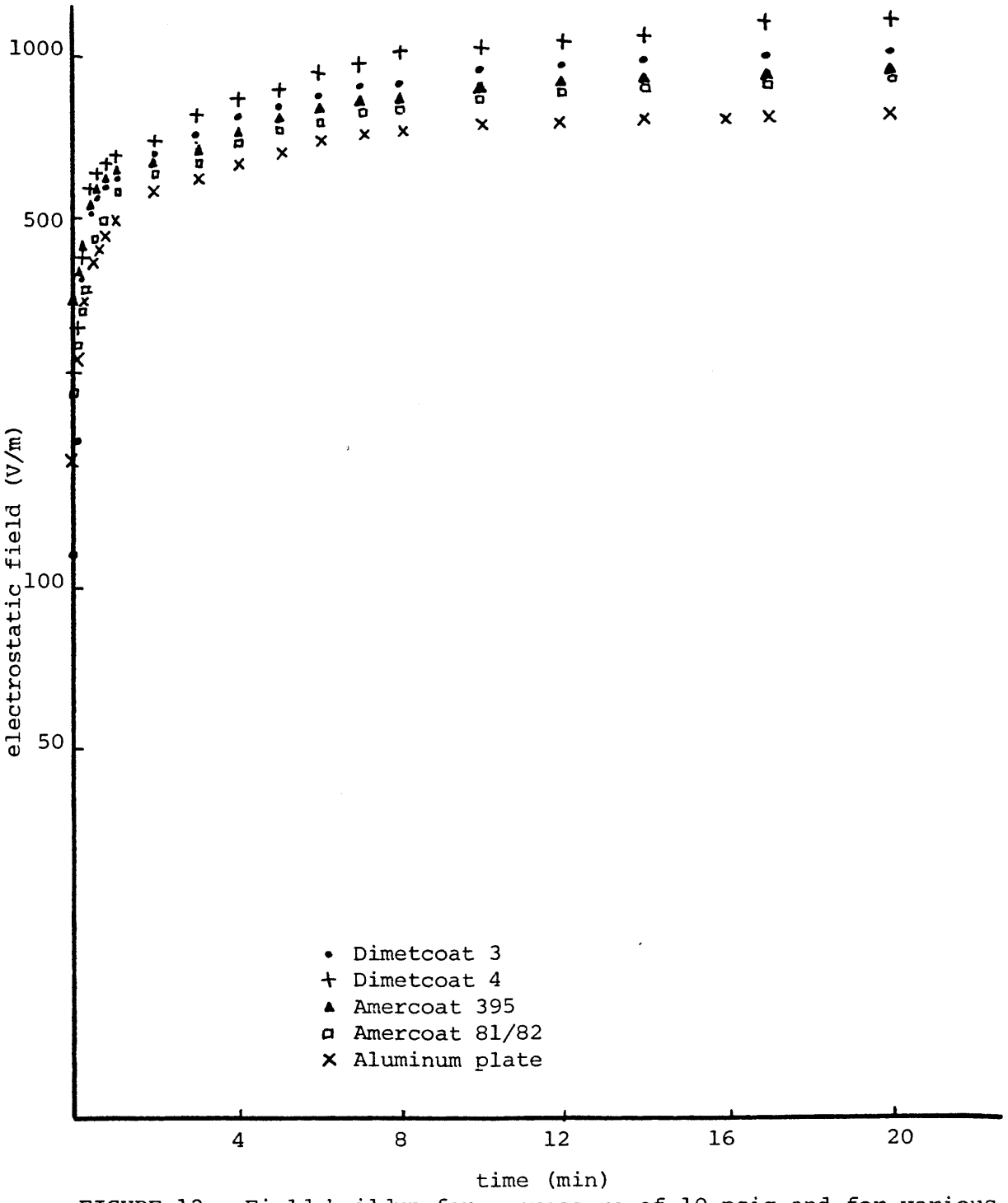

FIGURE 12: Field buildup for a pressure of 10 psig and for various materials used to coat the hanging plate

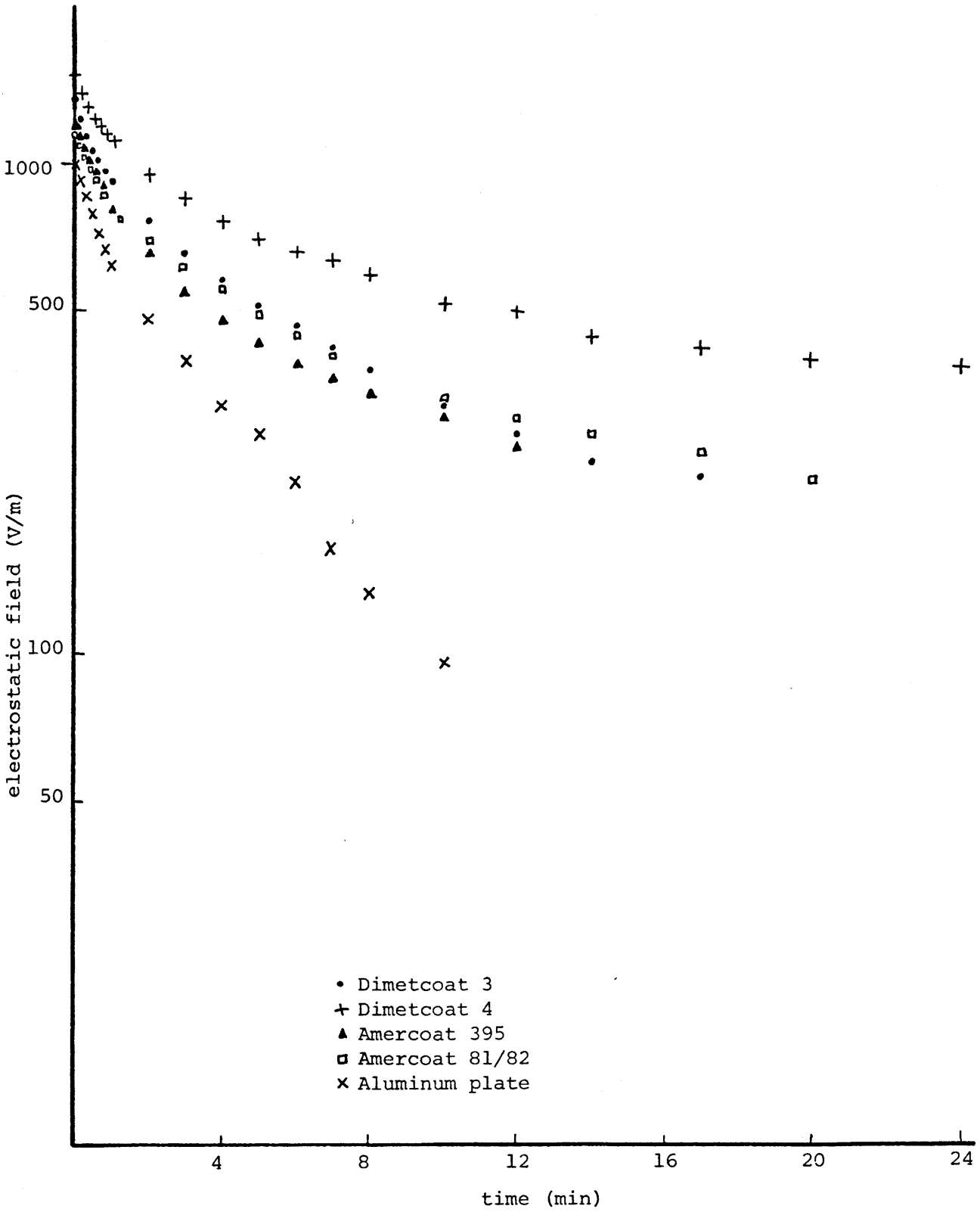

FIGURE 13: Field decay for a pressure of 10 psig before shutoff and for various materials used to coat the hanging plate

F. Temperature

Even though temperature was studied only indirectly, it seemed to influence the generation of the electrostatic field. For days when the atmospheric termperature was around 60°F smaller fields were measured when compared with those observed at temperatures of 80-90°F. The water temperature and the temperature inside the tank were not determined and hence it would be unreasonable to draw any conclusions as to the degree by which the field is affected. However, it is true that changes occur with varying temperature.

G. Estimation of the Electrostatic Field Inside a Rectangular Metal Tank

Electrostatic charge, which is produced by the motion of fuel through pipes, is carried into fuel tanks. If the magnitude of the field reaches an upper limit, which is 30,000V/cm for air, a discharge will occur and will therefore initiate an explosion if the composition of the fuel-air mixture is inside the explosive range.

The electrostatic field throughout a rectangular metal tank partially filled with a uniform charged liquid has been calculated when using the following assumptions:

1. The charge is homogeniously distributed;
2. The surface of the liquid is parallel to the bottom of the tank;
3. The boundaries of the tank are at earth potential.

The approximate expression proposed for practical calculation of the greatest field (the potential function in the tank is described as a doubly infinite Fourier series) existing in the vapour space of a rectangular tank is:

$$E_{max} = \frac{16\rho\ (\cosh\beta d - 1)\cosh\beta p}{\varepsilon_0 \pi^2 \beta\ (\varepsilon_V \cosh\beta p\ \sinh\beta d + \varepsilon_L\ \sinh\beta p\ \cosh\beta d)}$$

where

a,b,c are the length, width and height of the tank respectively

$$\beta^2 = \pi^2 \left(\frac{1}{a^2} + \frac{1}{b^2} \right)$$

d = depth of liquid measured from the bottom of the tank
p = depth of vapor = c-d
ρ = charge density of the liquid fuel
ε_V, ε_L = dielectric constants of fuel and vapour respectively, taken for purposes of calculation to be $\varepsilon_V = 1$, $\varepsilon_L = 2.2$

Considerable difficulty exists when attempting to calculate experimentally the magnitude of the electrostatic field inside the tank. This happens because any instrument projecting into the tank distorts the field. One way of avoiding this is by the use of the following formula:

$$|E|_{max} = |E|_{measured} \cosh\beta p$$

where $|E|_{max}$ = is the maximum field in the tank and $|E|_{measured}$ the measured field existing at the center of the roof of the tank.

In certain cases the fields produced by charged mists, i.e. water, can be as big as those produced by charge found in liquid fuel.

The field present in the vapour space of a cubical tank of side a when the tank is filled uniformly with a mist having a charge density ρ_1 is presented below.[15]

$$E_x = \frac{64a\rho_1}{3\varepsilon_o\pi^4} \cos\pi\frac{x}{a} \cos\pi\frac{y}{a} \sin \pi\frac{z}{a}$$

This practical expression can be found when calculating the potential from Poisson's equation and taking only the first terms of the series obtained by differentiating this potential. The greatest field existing in the mist is at the centre of each wall of the tank and of magnitude:

$$E_{mist} = \frac{64a\rho_1}{3\varepsilon_o\pi^4}$$

Hence the space charge density assumed to be uniform can be estimated from:

$$\rho_1 = 4.0 \times 10^{-11} \frac{E_{mist}}{a}$$

The above relationship can be applied to obtain an approximate value for the space charge created in a cargo tank. We can obtain a by assuming that a^3 is equal to the volume of the tank under consideration. Figure 14 shows charge density values obtained at the maximum field for a number of flows. It can be seen that ρ_{max} varies linearly with pressure for the range of flows examined.

If we have a conducting spherical container filled with a uniform space charge of density ρ (coul/m^3), the field E_r (volts/m) as a function of the distance r (m) measured from the center of the sphere is found to be[16]

$$E_r = \frac{r\rho}{3\varepsilon_o}$$

where the permitivity of free space $\varepsilon_o = 8.85 \times 10^{-12}$. When comparing the field inside a sphere with that of a cubic tank containing the same space charge density ρ, we find that for equal cube and sphere volumes $E_{cube} = 1.05E_{sphere}$, while for equal cubical side length and sphere diameter the relationship becomes $E_{cube} = 1.31\ E_{sphere}$.

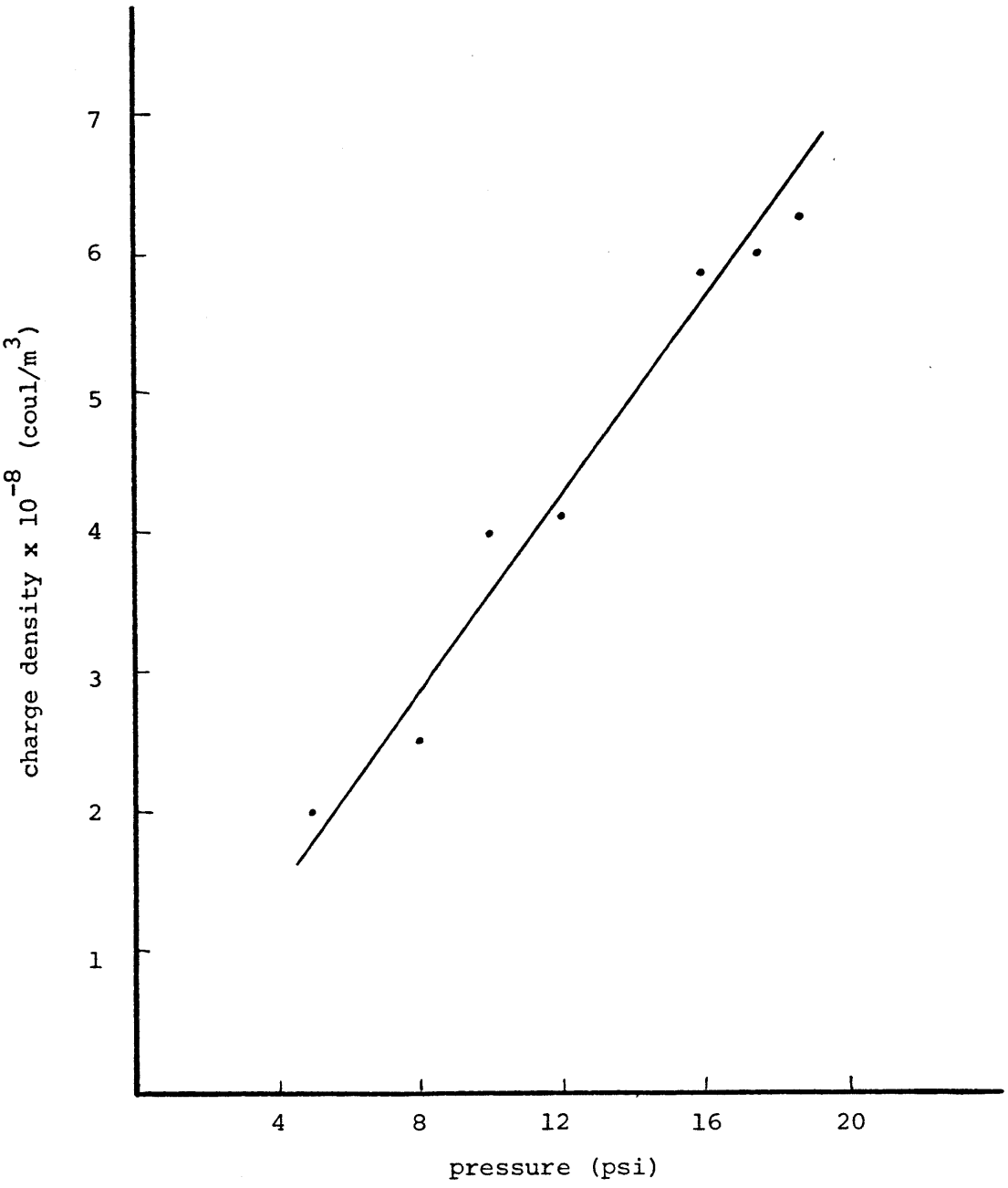

FIGURE 14: Charge density obtained at the maximum field vs. water pressure measured at the spraying nozzle

H. Comparison of Results

Different investigators have measured fields from which we can calculate the charge density ρ and construct the following table:

	Effective Length (m)	Peak Field (V/m)	Charge Density (C/m^3)
Bathroom (tap water)[8]	2.5	-600	-7.7×10^{-9}
Cargo Tank (seawater)[8]	30	+20,000	$+2.1 \times 10^{-8}$
Cargo Tank (seawater)[13]	34	+250,000	$+2.55 \times 10^{-7}$
Cargo Tank (tap water)[13]	34	-150,000	-1.41×10^{-7}
Cargo Tank (seawater)[6]	22.9	+700,000	$+3.8 \times 10^{-7}$
Model Tank (tap water)	1.36	-2240	-6.6×10^{-8}

We obtain the effective length by assuming that the cube of the effective length is equal to the volume of the container. From the above table we see that the charge densities measured in some cargo tanks differ by a factor of 3 to 4 from those measured in our model tank. However, while a setup with the field meter situated at the top of the tank might produce satisfactory results for measurements taken in a tank filled with charged mist, this method is hindered in practice by the presence of steel structures such as girders and stringers. Thus, it has become established practice to lower the field meter attached to a steel cable into the tank. This in turn affects the field present in the tank and due to a localized high field false measurements result.

Hence, we can conclude that, since the order of magnitude of the space charge is 10^{-8} coul/m^3, the charge density present in a tank must be more controlled by processes in the atmosphere of the container rather than by the container dimensions.

CHAPTER V

Summary

The observations which were analysed in the previous part can be summarized as follows:

1. When a tap water jet hits an obstacle strong electrification develops which gives rise to a negative field.

2. Both the charging rate and the maximum steady-state value of the field produced by the impinging water jet increased with increasing flow rate.

3. Decay rates are governed by the magnitude of the field being faster for larger fields.

4. Grounded narrow objects penetrating up to half way across do not substantially change the character of the field at the opposite wall. A grounded sphere located 2/3 the tank height from the wall reduced the wall field by about 20%.

5. Appropriate ventilation can help keep the peak value of the field down and accelerate overall decay time by as much as 500%.

6. Both the field and the charging and decay mechanisms appear to be affected by temperature changes.

7. Organic and inorganic surface coatings which are commonly employed to cover the inside of tanks carrying petroleum products had little effect on the value of the peak field or the decay time when used as target surfaces for the water jet.

8. The space charge present in a tank is controlled by the atmosphere inside the container rather than by the container dimensions.

CHAPTER VI

A. Explosion Fundamentals

The material in this part is intended to give the reader a feel for the development of a combustion wave from a source of electrical ignition. The term "explosion" is used to denote any uncontrolled and undesired combustion.

Concerning spark ignition, assume that a point source of energy imparts W_e joules to a small volume of a combustible mixture. At the site of the energy discharge the local temperature rises far above the ignition temperature of the mixture and a small kernel of the mixture ignites. The temperature within the small volume decreases rapidly due to conduction and radiation, thus causing loss of energy to the surrounding unburned gas. The gas layer surrounding the initially ignited kernal is in turn raised to its ignition temperature and chemical reaction occurs, so that a combustion wave is formed which propagates outward with approximately a spherical symmetry.[17,18]

B. Lower Explosive Limit and Upper Explosive Limit

If, using a specific ignition source, one determines the critical energy required to ignite various concentrations of a fuel-air mixture, curves such as the one shown in Figure 15 are obtained.[18] As concentration changes away from that at which the least amount of energy is required for ignition, the energy required to ignite the mixture increases, thus becoming infinite at the two concentrations to which the curves are assymptotic, the lower explosive limit, L.E.L., and the upper explosive limit, U.E.L. It is believed that heat absorbed by the unburned gas is responsible for the flame quenching in such limit mixtures. The complete flammability envelope is described not only by the hydrocarbon concentration but by the oxygen content of the mixture as well. Below certain limiting oxygen concentrations, combustion cannot be supported. Limiting oxygen concentrations for aliphatic hydrocarbons are reported as 11.0 percent with nitrogen as the diluent gas and 13.4 percent with carbon dioxide as the diluent.

It appears that convection and radiation currents are generated, which are capable of quenching the flame, because of the low burning velocity of the combustion wave. From Figure 16 one can observe that as the concentration of the fuel-air mixture approaches either the L.E.L. or the U.E.L., the burning velocity of the combustion wave decreases substantially, the lowest value being 0.4 of the highest. The results are taken from tests conducted on a benzene-air mixture, for a 0.5 cm electrode gap.

For the range of mixtures which support combustion, the amount of energy added by combustion and the thermal conductivity and thermal capacity of the mixtures are different. All these have an effect on the

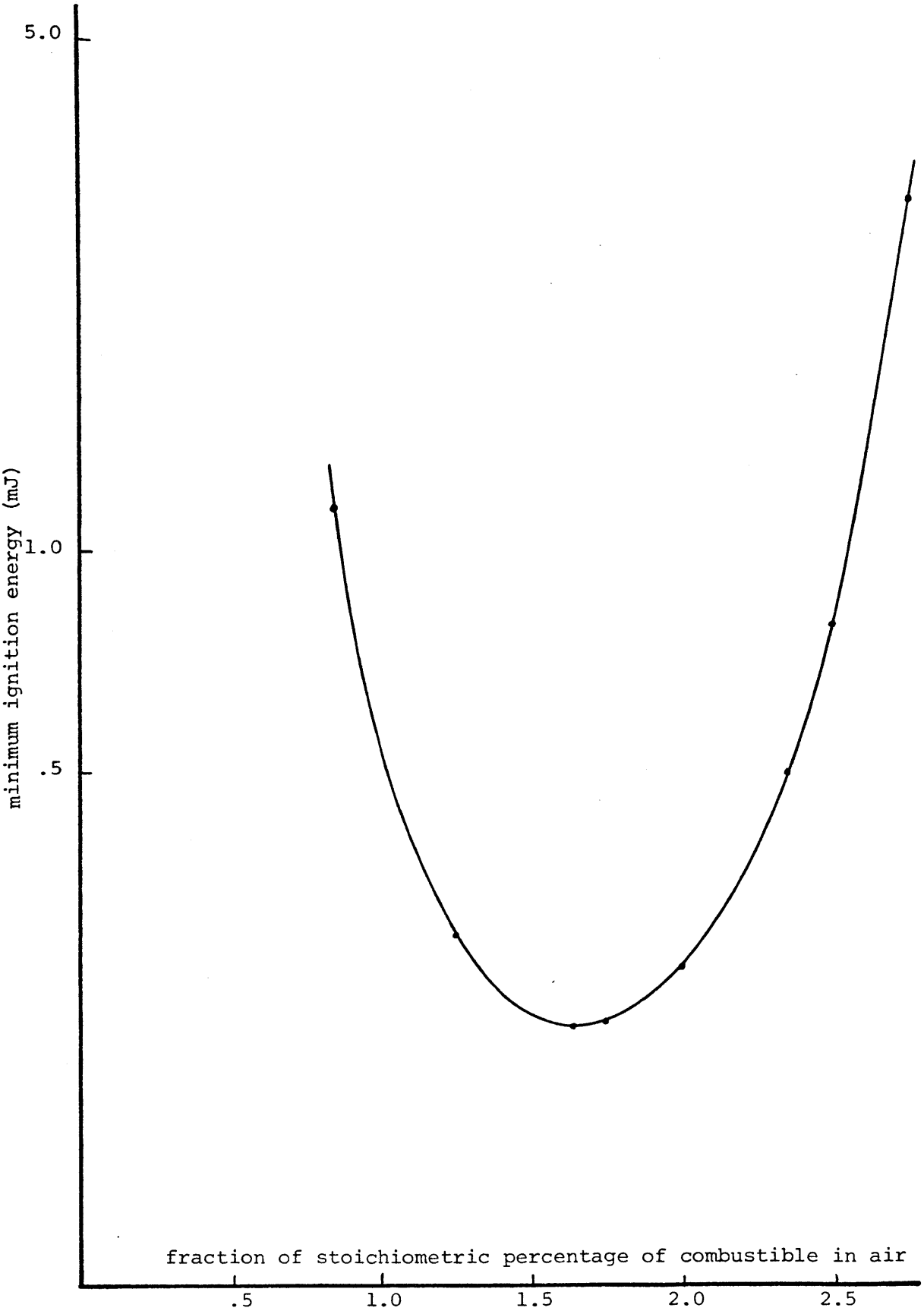

FIGURE 15: Minimum ignition energies for a benzene air mixture

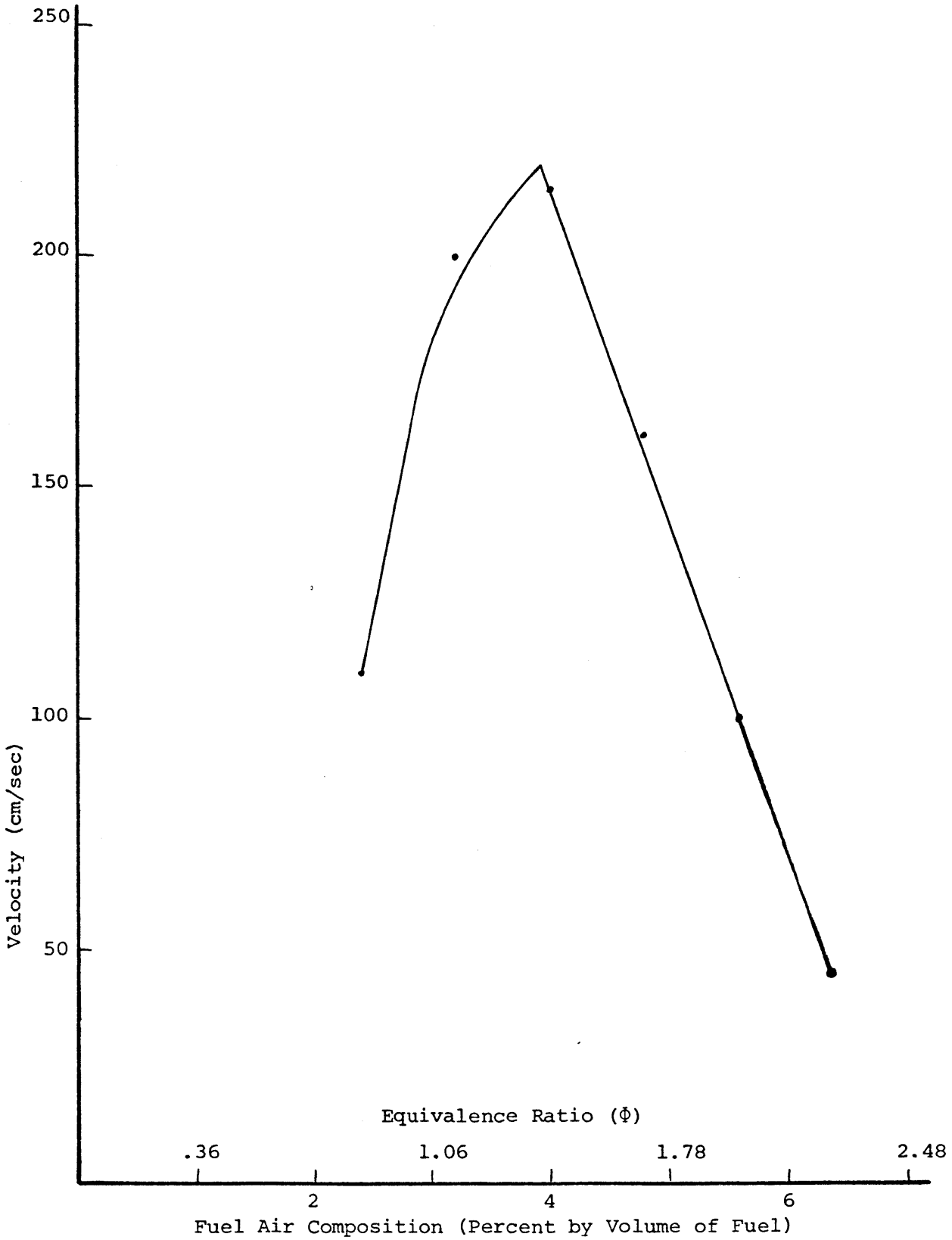

FIGURE 16: Flame velocity vs. fuel air composition

flame velocity, which is in turn related to ignition energy. Figure 17 shows the correlation between ignition energy and flame velocity.

When combining these observations, one immediately deduces that indeed the ignition energy increases rapidly as we move away from the most easily ignited concentration of the fuel-air mixture, thus becoming infinite at both the lower and upper explosive limits.

The lower and upper explosive limits are fairly constant for a particular gas-air mixture, with only a slight variation depending on the way of propagation of the combustion wave (upward, horizontal, downward).

Crude oils carried by tankers consist of several gas compositions, which can be found from crude oil analyses. For each of these compositions the L.E.L. and U.E.L. can be calculated by use of the modified Le Chatelier expression:

$$L_m = \frac{100}{\frac{C_1}{L_1} + \ldots + \frac{C_n}{L_n}}$$

where L_n is the explosive limit (either L.E.L. or U.E.L.) as percent by volume, $C_1 \ldots C_n$ is the concentration of the individual hydrocarbon component in the mixture, as percent by volume and $L_1 \ldots L_n$ is the explosive limit for the individual hydrocarbon component, as percent by volume.

From the point of view of explosion hazards to fuel spray combustion, the coarser aerosols maintain flame propagation at lower fuel-air ratios than fine aerosols or gaseous mixtures. This happens because coarse particles move randomly with respect to each other, while fine particles are firmly held in place by their air envelopes, thus communicating flame more readily.[18]

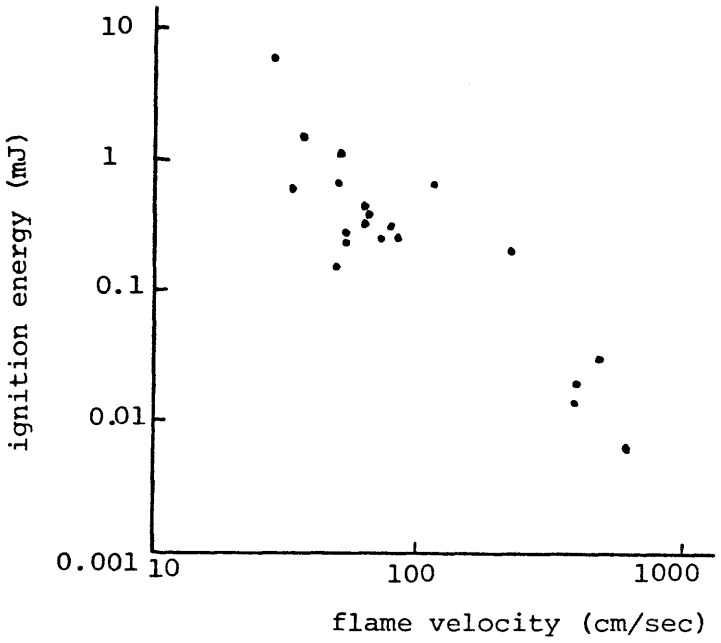

FIGURE 17: Relationship between ignition energy and flame velocity in 2.5 cm tube

CHAPTER VII

A. Experimental Procedure

An apparatus and experimental procedure is described in this section for performing explosions under controlled conditions. The pieces constituting the explosion chamber are so designed as to combine both high precision in measurements as well as ease in obtaining data and observing various phenomena. Because the apparatus used is not standard, every part is described in detail.

Test Bomb

The chamber where the explosions were carried out consisted of a cylindrical vessel, 10.04 cm I.D., 12.63 cm O.D. and 5.95 cm height. It was made out of lucite and mounted between two aluminum plates, which served as electrodes. Lucite was chosen as the appropriate material for constructing the chamber because of its high mechanical strength (tensile strength between 7,000 and 11,000 psi), its electrical insulating capacity and its excellent clarity which helps the experimenter observe what takes place prior and during an explosion. It is essential that the chamber be made out of an electrically insulating material, so as to create a potential difference between the two electrodes and hence create a spark which would ignite the fuel-air mixture. A small hole drilled on the side of the test bomb allows fuel to be injected by means of a microsyringe.

The cylinder is compressed between the electrodes by means of six 1.27 cm diameter nylon rods. In order to ensure that the spark occurs inside the chamber and to prevent discharges along the insulator surfaces the upper plate extends into the chamber as shown in the following picture, Fig. 18, which shows the chamber assembled and ready for test.

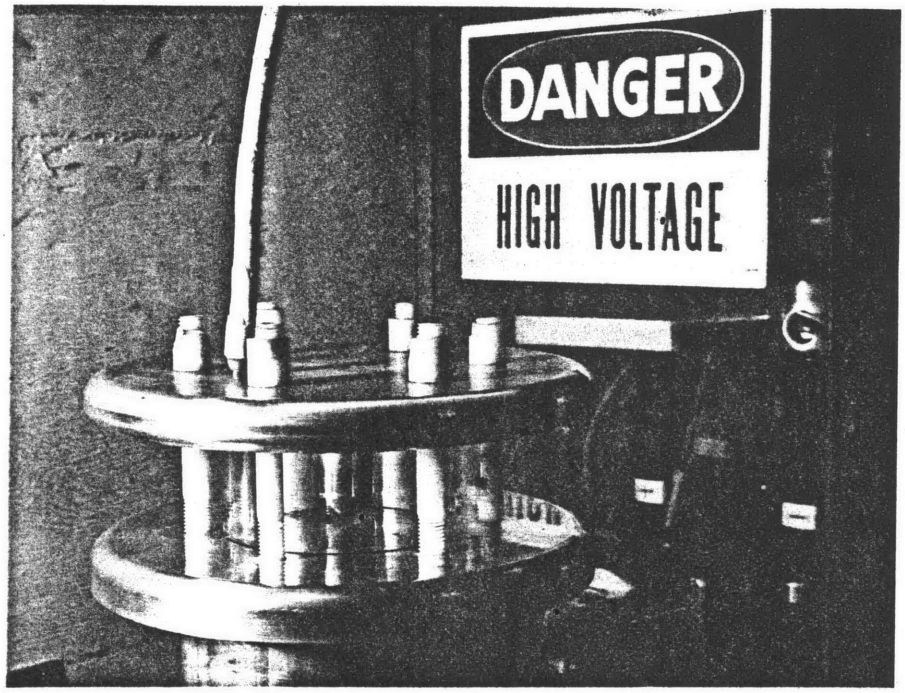

FIGURE 18: The test chamber

This extension is a rod, hemispherical at one end, threaded to the upper plate. By controlling the number and length of cylindrical washers between the extension electrode and top plate the gap length can be set accurately to the values chosen for study.

Electrodes

In an effort to investigate the effects of electrode shape and material in altering the ignition characteristics as well as the breakdown voltage, two different shapes were examined. As mentioned earlier, one was the solid aluminum rod of 3.17 cm diameter which is hemispherical at one end and the other a 0.12 cm diameter steel wire. These are both shown in Figure 19.

Different tests of breakdown voltage using the hemispherical electrodes were conducted. It was observed that whereas the effect of fingerprints and general electrode cleaningless was insignificant, the contour was important. By using a smooth electrode free from sharp edges, we were able to minimize corona-type discharges and to obtain reproductible results for any gap. The effect of electrode material on the breakdown voltage is discussed in a later part.

Pressure Measurements

A pressure transducer of the Kistler 609 pizoelectric type with maximum sensitivity of 1 psi was mounted in the bottom aluminum plate 3.3 cm from the axis of the electrodes and not directly beneath the upper electrode tip, so as to avoid any discharges to it. The transudcer made possible recordings on an oscilloscope of pressure versus time from spark breakdown till after the explosion. To avoid false readings, the connections between the transducer and the oscilloscope were kept clean with a Freon spray.

The following picture Figure 20 shows a pressure recording for the case of a spark discharge in air with the transducer located 1.1 cm from the electrode axis. The pressure wave is seen to arrive at the transducer after a delay of 40 microseconds which is due to the time for sound to travel the distance to the transducer.

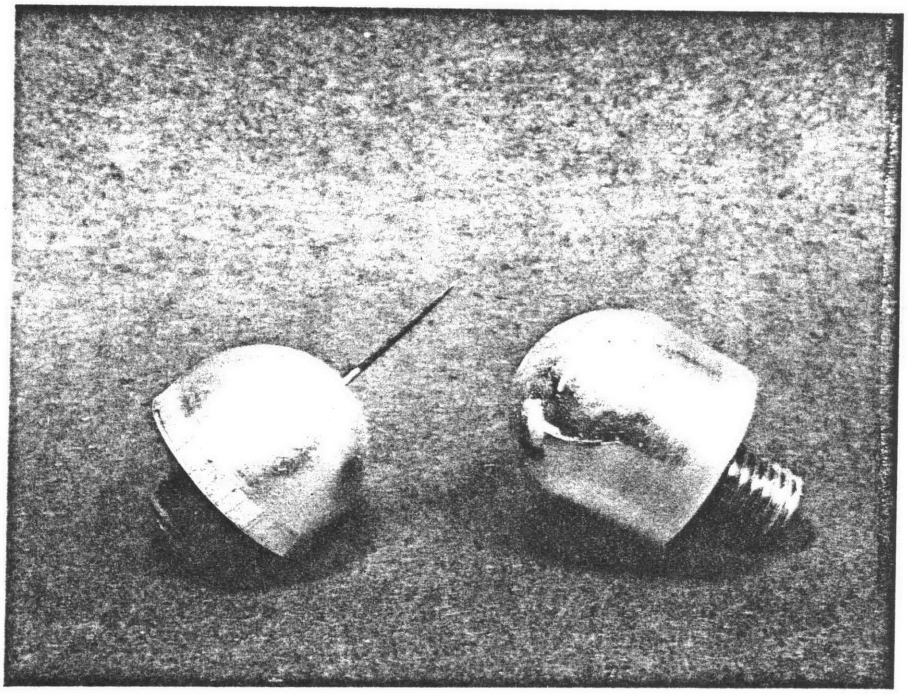

FIGURE 19 Aluminum hemispherical electrode and steel wire electrode

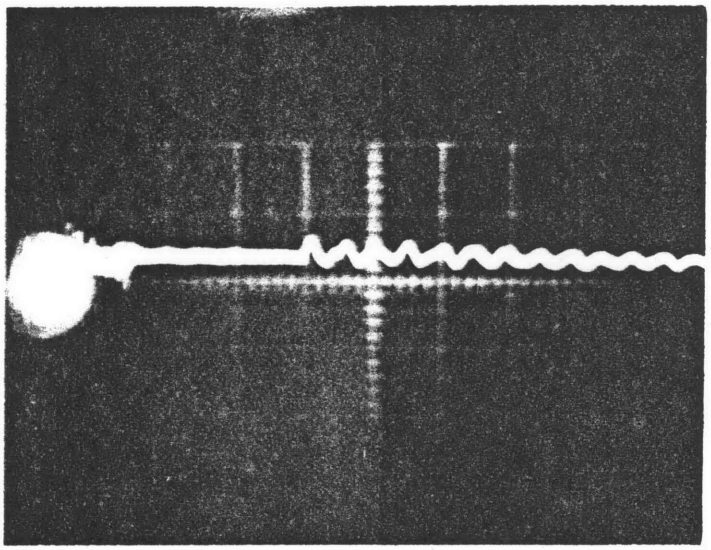

FIGURE 20 Pressure vs time for spark discharge in air, for 1 cm gap
Vertical calibration: 1 box division = 50 psi
Horizontal calibration: 1 box division = 10 microseconds

B. Procedure for Ignition Tests

The spark electrodes are adjusted accurately to the desired gap and are carefully cleaned. The bomb is then flushed with dry air at 15 psi for 2-3 minutes. Usually this length of time is sufficient to remove the combustion products of the previous explosion as well as any moisture present. The hole used for the deposition of the fuel is covered with plastic tape and liquid fluid is introduced by means of a high precision microsyringe. In this way the desired percent by volume of fuel-air ratio is achieved to within one percent. The fuel is then allowed sufficient time to evaporate. After the last droplet of fluid has disappeared from the bottom electrode, the high-voltage power supply is turned on. The electrode is then slowly charged and the breakdown voltage at which the spark occurs is observed. The pressure wave is recorded on the oscilloscope and is automatically photographed. After the explosion the test bomb is again flushed with dry air and is ready for subsequent use.

When performing tests for the determination of the minimum energy required to ignite fuel-air mixtures for a particular gap, the capacitance of the spark circuit is adjusted. This is achieved by means of capacitors added in parallel.

The smallest value of the capacitance goes to the lower limit of 17 micromicrofarads, which is the capacitance of the test bomb itself. Where necessary power supply and connecting cable capacitance was isolated from the test bomb by a series 10^9 ohm high-voltage resistor. A micro-ammeter (0-30μA and 0-300μA) was used to measure corona-currents prior to spark breakdown. Currents were observed before breakdown when the

wire electrodes were used and for gaps greater than 1 cm.

The fuel used to study the various mechanisms of ignition and to analyze the results of the explosion tests was benzene. It was felt that similar results would be obtained by using various crude oils and their components which are transported by tankers.

CHAPTER VIII

Results and Discussion

A. Breakdown Voltage Measurements

It is known that the breakdown voltage in atmospheric air occurs when a field E = 30,000 V/cm is reached. This value is measured between two flat electrodes which are separated by a distance of 1 cm, becoming larger for smaller gaps and smaller for larger gaps. One of the earlier thoughts concerning the experiment was to investigate the breakdown voltage inside the test chamber when only air was present, for different gaps. Figure 21 shows the results of using steel and aluminum hemispherical electrodes. One can immediately see that for the 1 cm gap the breakdown voltage is below the expected 30,000 volts. This is due to the geometrical shape of the upper electrode. However, for our particular case the field is somewhat non-uniform. We can determine the maximum field E_{max} by use of the following formula:[19]

$$E_{max} = \frac{V}{g}\left[\frac{\frac{2g}{r} + 1 + \sqrt{\left(\frac{2g}{r} + 1\right)^2 + 8}}{4}\right]$$

where g is the gap between the hemispherical and the flat electrodes, V is the value of the breakdown voltage and r the radius of the upper electrode. Figure 22 shows the normalized results. As it can be seen, the values that are closer to that for the atmospheric field are the ones calculated for the smaller gaps, namely 0.25 cm and 0.5 cm. The large deviations observed for the larger gaps are due to the nonuniformity of the field created by the presence of the lucite chamber which acts in a way to distort the field.

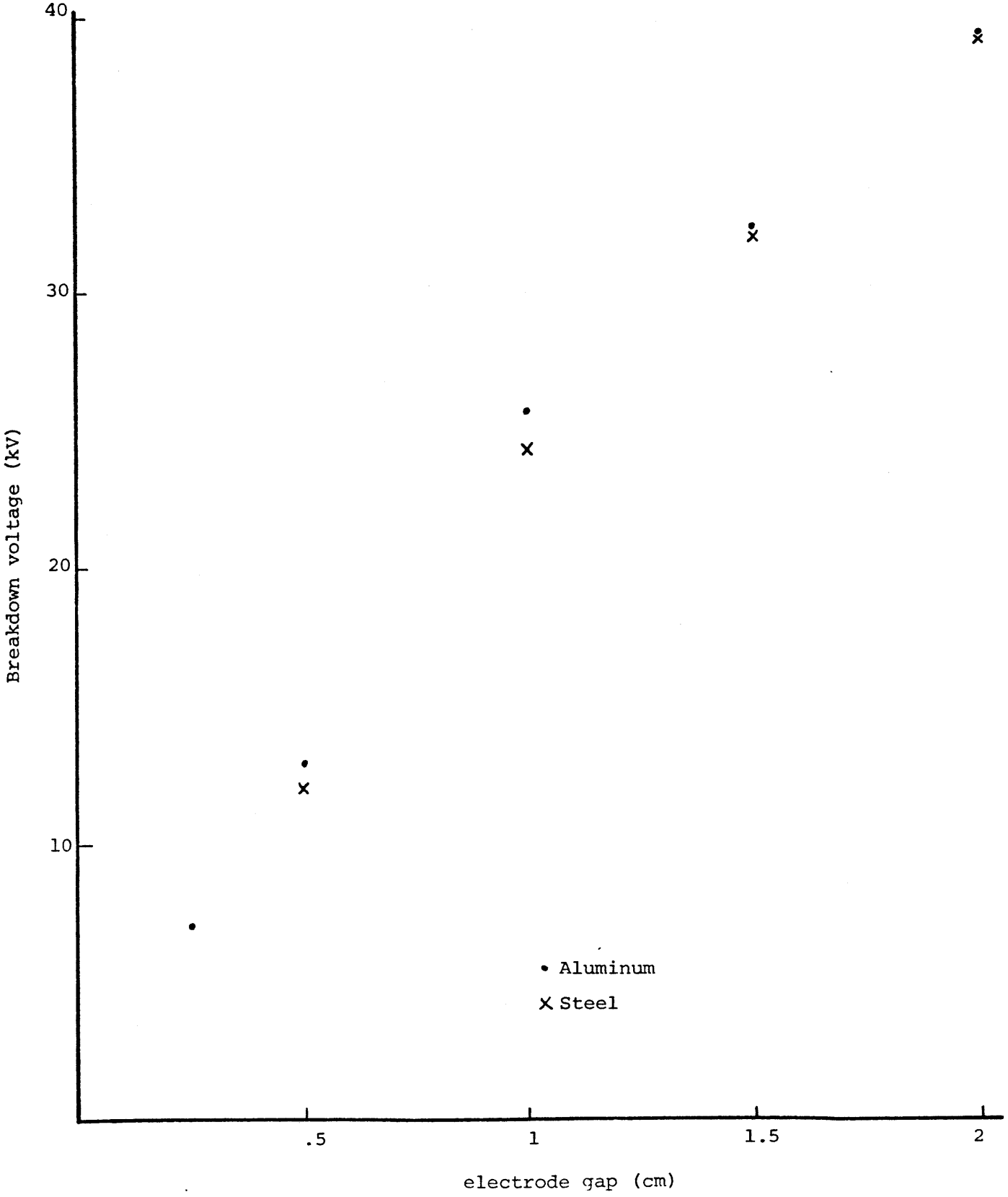

FIGURE 21: Breakdown voltages versus electrode distance for steel and aluminum hemispherical electrodes

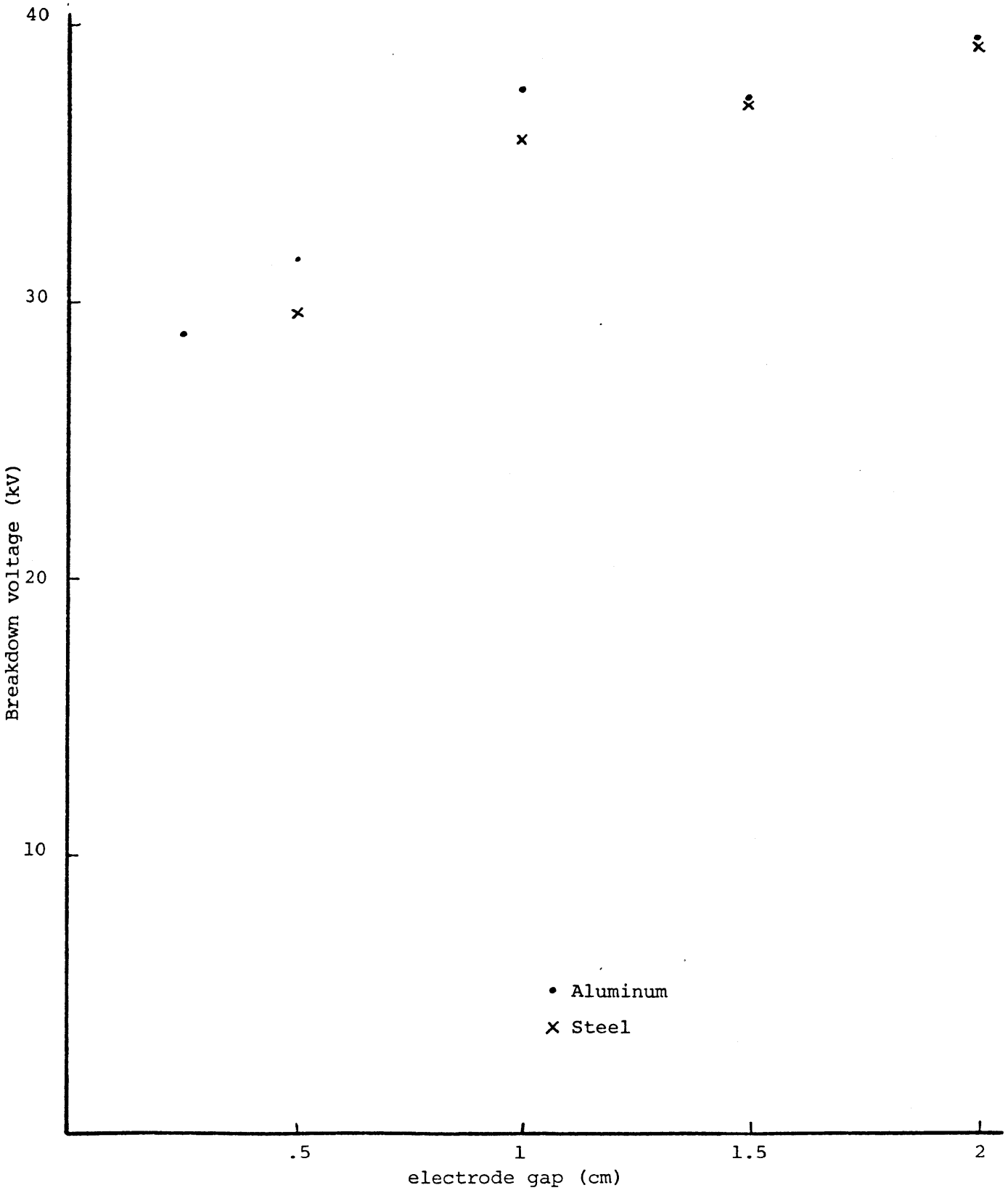

FIGURE 22: Normalized breakdown voltages versus electrode gap for steel and aluminum hemispherical electrodes

Breakdown voltages for the same gaps when benzene was introduced, were also measured. It is interesting to note that for the same gap the voltage was somewhat lower. The fuel-air composition did not affect the breakdown voltage, the values being uniform in the entire explosive range. Figure 23 shows the results obtained when benzene is present as well as those when water is also introduced in addition to the fuel. Again, whater acts in a way to lower the voltage under consideration.

In an effort to detect any corona type discharges, the currents prior to the spark were also measured. For small gaps no currents were found prior to the spark, while for the 1 cm gap, the current starts rising when the applied voltage becomes 20 kV to finally reach a maximum value of 1.7μA just before ignition occurs.

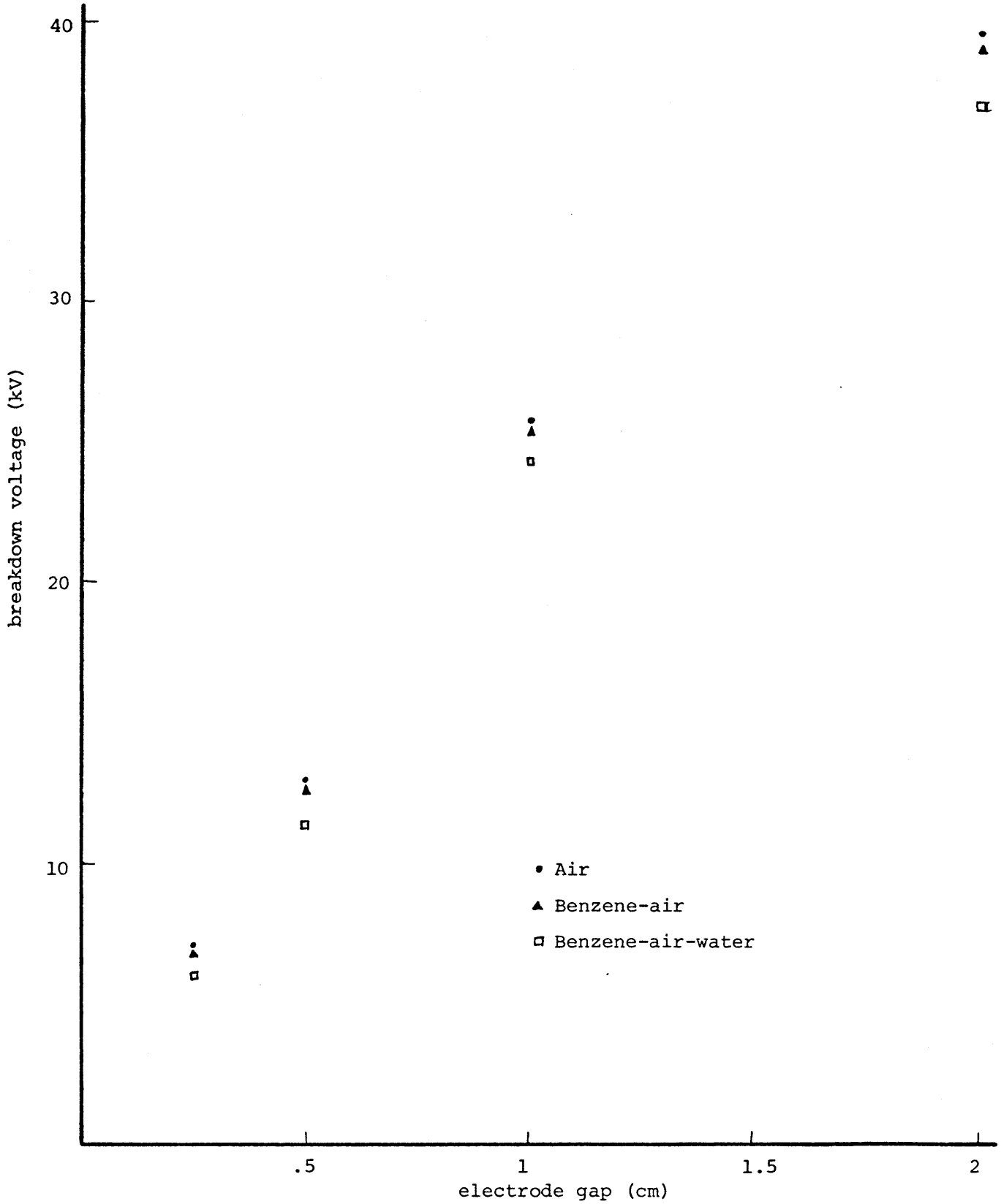

FIGURE 23: Breakdown voltages vs. electrode gap for air, benzene-air, and benzene-air-water mixtures

B. Wire Measurements

The material presented in this part is intended to help the reader gain a better qualitative understanding of the processes of ignition by electric arcs, so that ignition data can be better interpreted.

During the initial application of voltage, electrons normally present in the gap, due to collision of cosmic rays with gas molecules or the electrode material, are drawn to the anode. As the potential between the electrodes increases, electrons are given a velocity component in the direction of the anode. At the critical potential called the breakdown voltage, the number of electrons produced by collision with other electrons, increases exponentially with the increased conductivity due to the large number of electrons in the gap, the voltage between the electrodes drops radically and breakdown is said to have occurred.[17]

Wires made out of different materials were examined for a variety of gaps. Figure 24 shows voltage-current curves for a tungstun wire with electrode spacing as a parameter. When plotted on log-log paper the data points fit on a straight line. If we do not take into consideration the lowest measurement, where the current increased rapidly with voltage, the following relationship can be deducted:

$$\log i = c \log V \text{ or } i = V^c$$

where i is expressed in μA and V in kV. The constant C ranges from 1.5 to 2 depending on the electrode gap. It is interesting to note that the current prior to breakdown reaches almost the same level and is independent of the electrode distance.

Another object of the wire electrode measurements was to see whether the fuel-air composition affected the current levels prior to

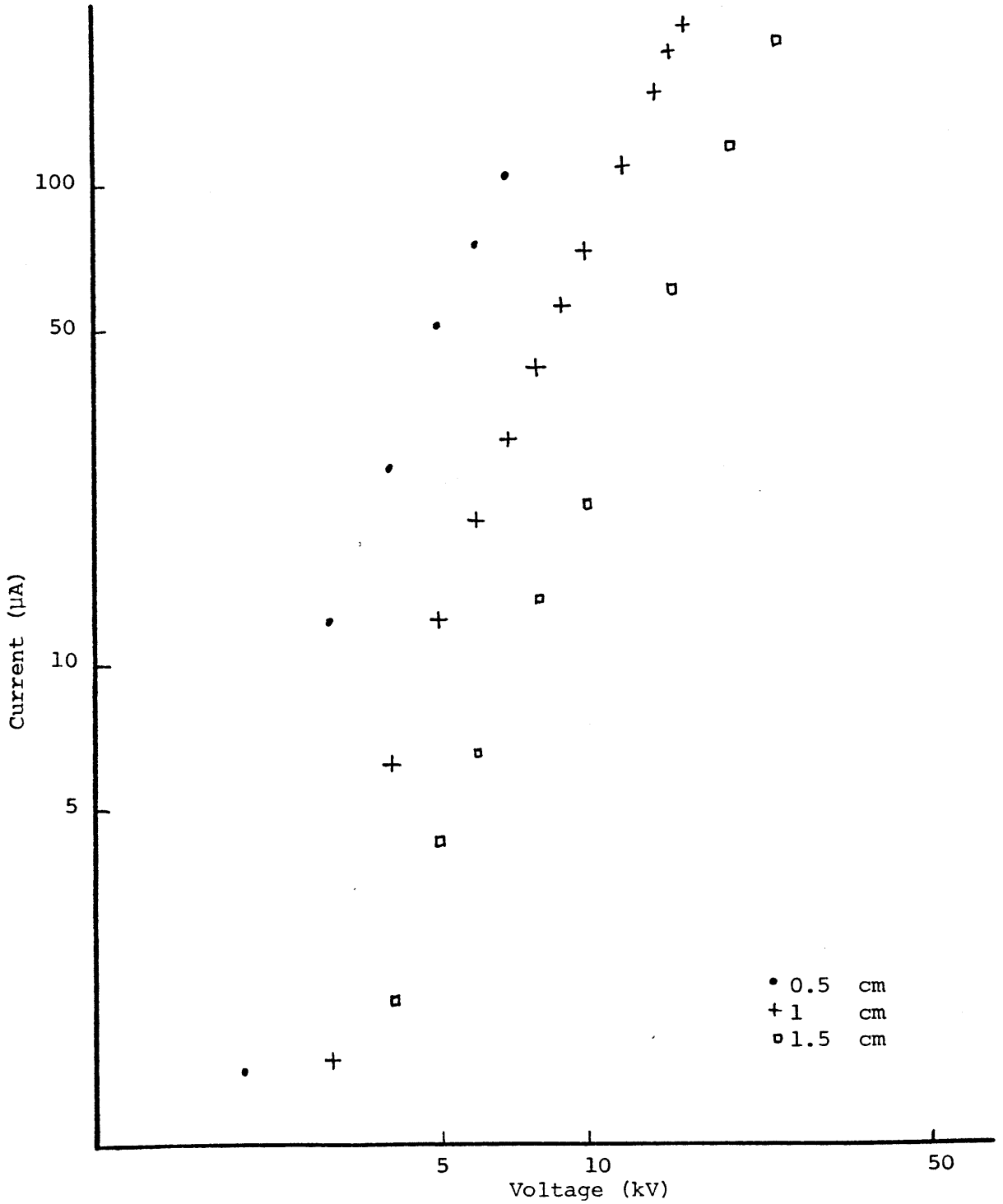

FIGURE 24: Voltage versus current for various gaps using a tungstun wire

breakdown. In tests conducted with the tungstun electrode and benzene-air mixtures no differences were observed for composition between 2.4 and 7.2 by volume of fuel. In Figure 25, which shows the results plotted on log-log paper, a test including measurements in dry air only is also included. As was the case with the hemispherical electrodes, here too benzene acts in a way to lower the current for a particular applied voltage. Further reductions in the level of the breakdown voltage, were also observed when water vapor at saturation was injected in addition to the fuel. In every case where corona currents were measured a blue glow in the vicinity of the tip was observed. The intensity of the light increased as current increased. The presence of the glow apparently was not in itself a cause for igniting explosive mixtures. On the other hand, explosions were always preceeded by spark breakdown when the fuel-air composition was inside the explosive range.

The above observations were also true for tests conducted when steel wires were used. One thing of interest was that for a steel wire, when only air was present in the chamber, the i-V measurements do not fall on a straight line as was the case with the tungstun wire but lie on a curve. Figure 26 shows this for a gap of 1 cm together with test results conducted with tungstun wire for comparison. In general, breakdown voltages seemed to be slightly higher for steel wires as can be seen from comparing different figures, the last measurement being that at which breakdown occurs.

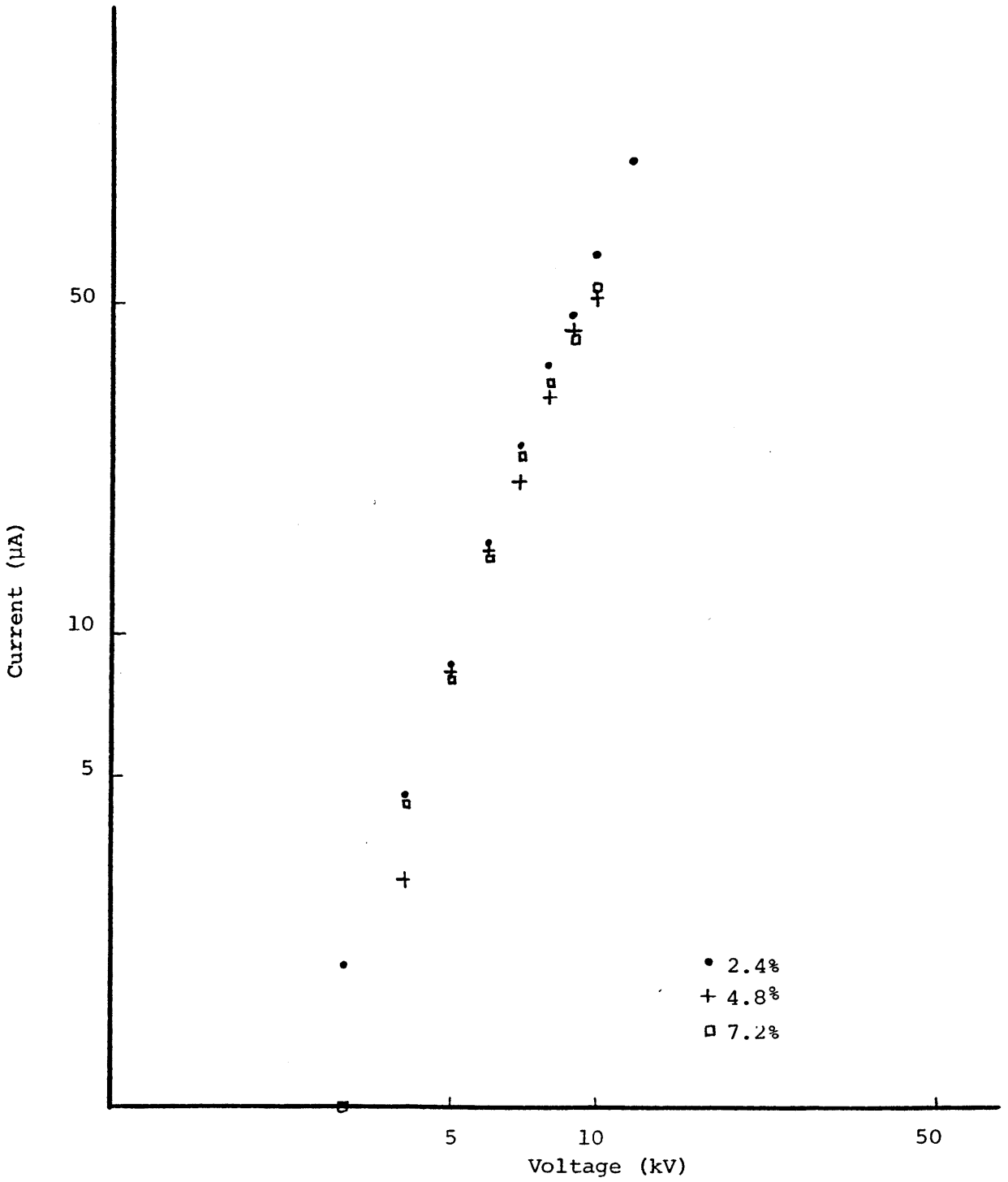

FIGURE 25: Voltage versus current for various fuel-air compositions as percentage by volume of fuel

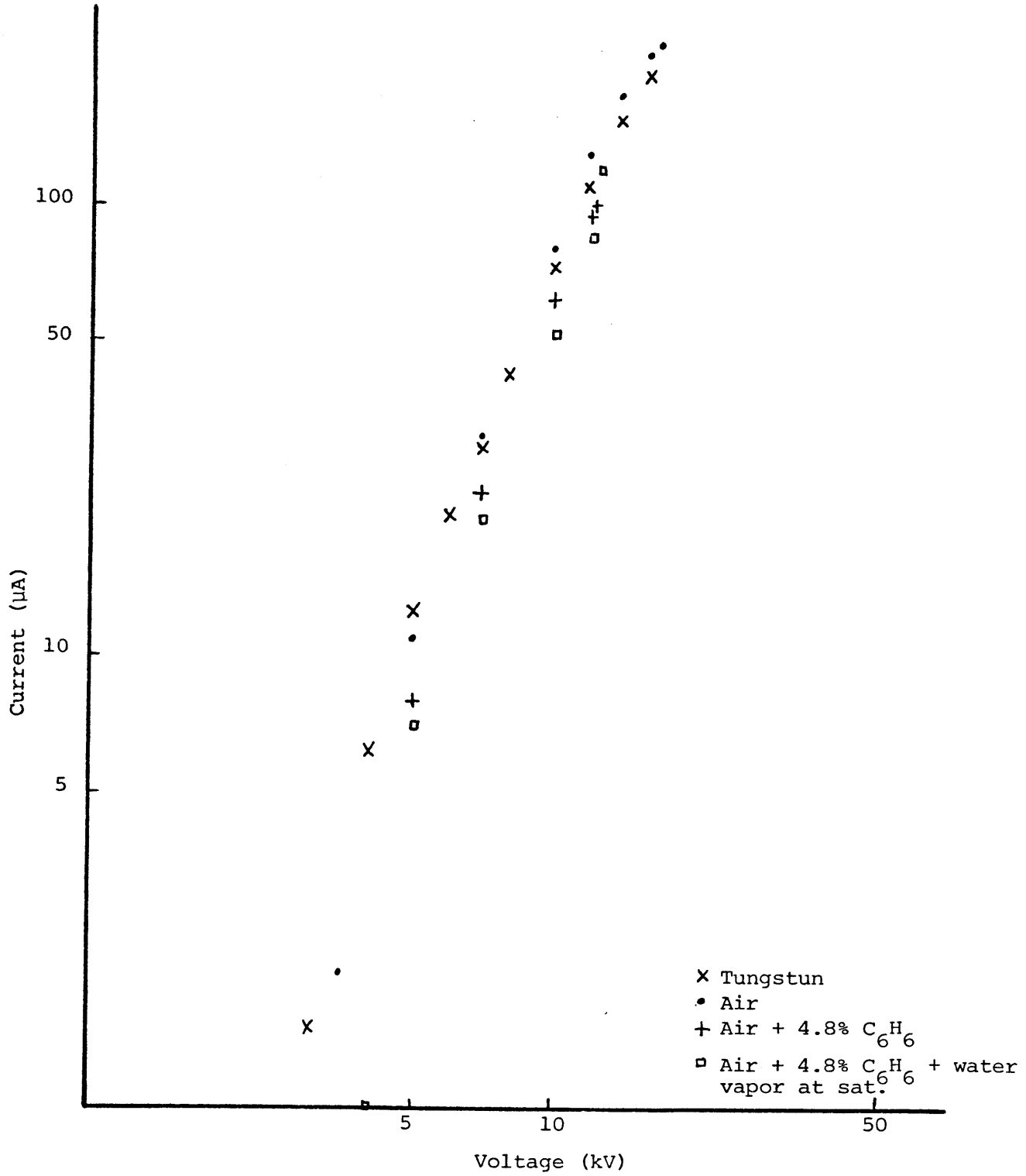

FIGURE 26: Voltage versus current for air, fuel-air and fuel-air-water using a steel wire

C. Pressure-time Record; Hemispherical Electrodes

Numerous tests were conducted to determine the pressure rise in the chamber due to the explosion of the fuel-air mixture contained in it. Having in mind a time-pressure record of an explosion, one would expect that the pressure would rise rapidly, reach a peak and then decline slowly to its initial value. However, in our particular experiment this wave-form was altered somewhat by the presence of gas escape holes.

In order to facilitate the discussion of the pressure record a number of photographs showing the recordings on an oscilloscope for various gaps using an aluminum hemispherical electrode are included. Figures 27, 28, and 29 show the results of explosions conducted with fuel air mixture compositions ranging from the L.E.L. to the U.E.L. Photographs of explosions throughout the explosive domain when water vapor at saturation was added in addition to the fuel-air mixture are also included. It is observed that indeed the pressure rises fairly quicly at the beginning up to a point and then the rate of pressure rise drops until the peak value is reached. This becomes more evident as the gap between the aluminum electrodes increases and can be more readily seen for the composition of 3.95% by volume of fuel. In fact at the 2 cm gap two pressure peaks exist. The peculiarity of the double pressure peak seems to be associated with the geometry of the test-bomb. As was explained at the beginning, the upper electrode extends into the explosion chamber. The flame wave, which is spherical in nature, is thus hindered from propagating uniformly throughout the vessel. As a result there still exists some mixture which has not been burned when the explosion wave reaches the exhaust valve (the hole through which the fuel is

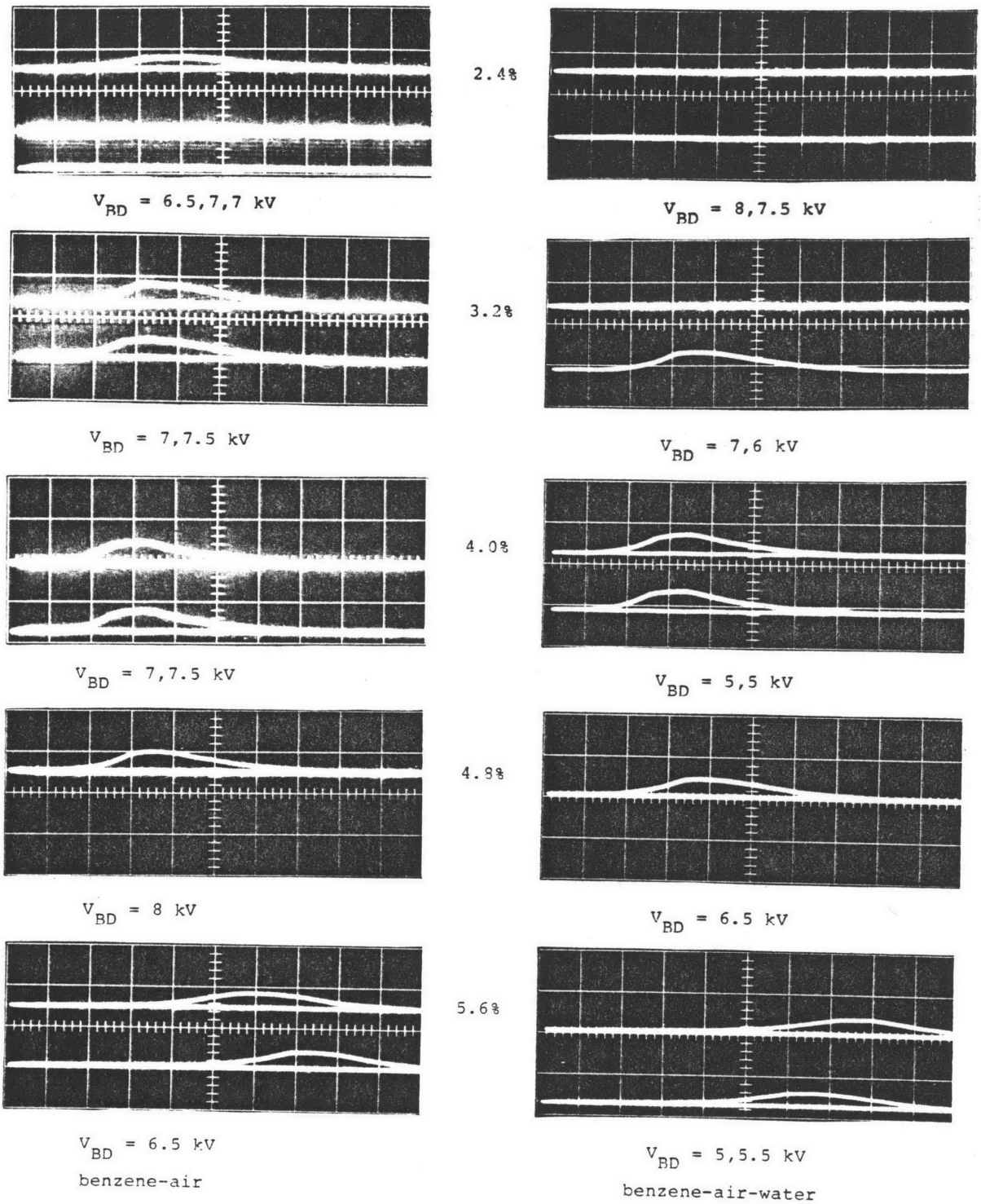

FIGURE 27: Pressure vs time for spark ignited explosive mixtures at 0.25 cm gap with 1.6 cm radius electrode.
Vertical calibration: 1 box division = 100 psi
Horizontal calibration: 1 box division = 10 milliseconds
Center column: fuel-air composition in % by volume of fuel

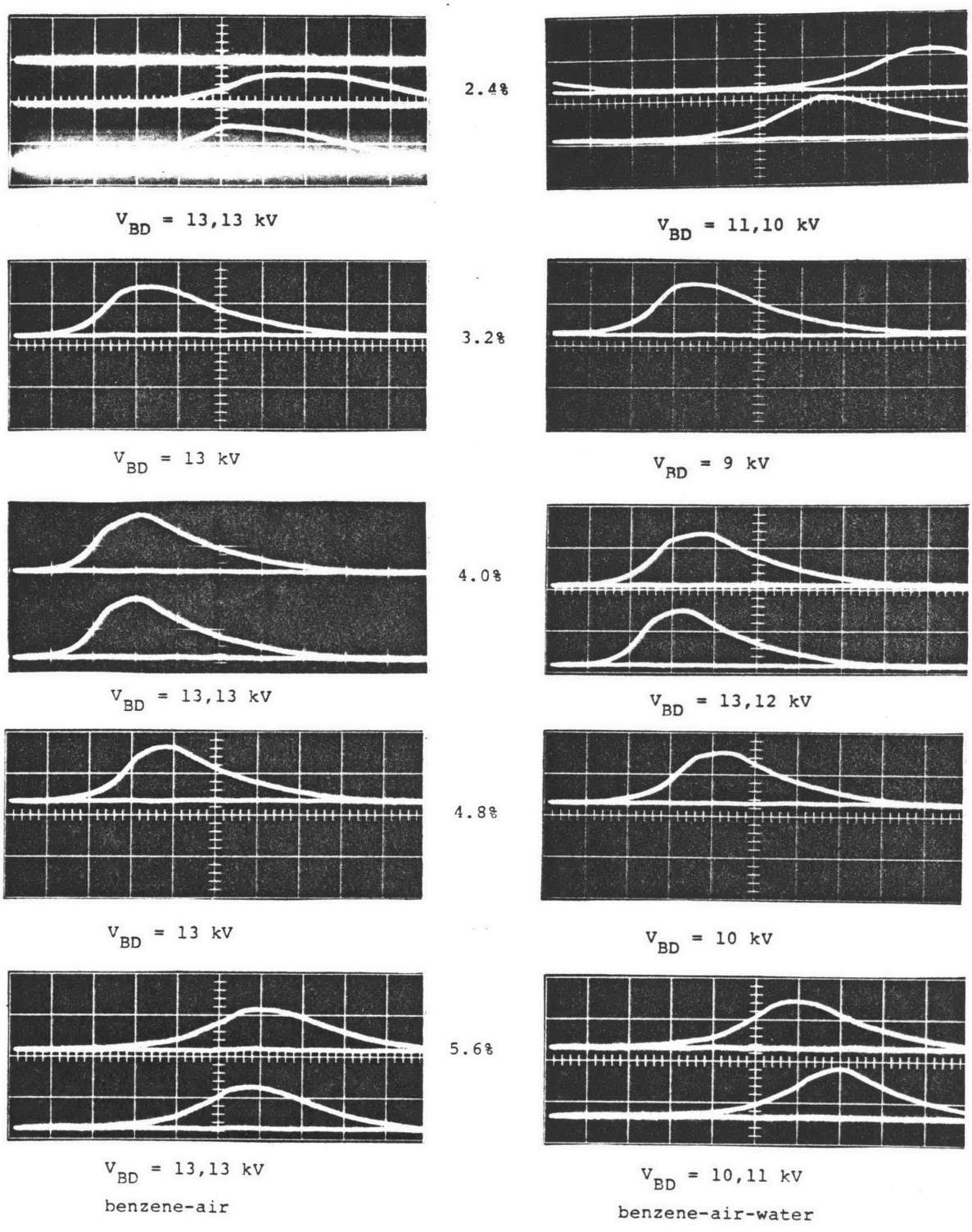

FIGURE 28: Pressure vs time for spark ignited explosive mixture at 0.5 cm gap with 1.6 cm radius electrode.
Vertical calibration: 1 box division = 50 psi
Horizontal calibration: 1 box division = 10 milliseconds
Center column: fuel-air composition in % by volume of fuel

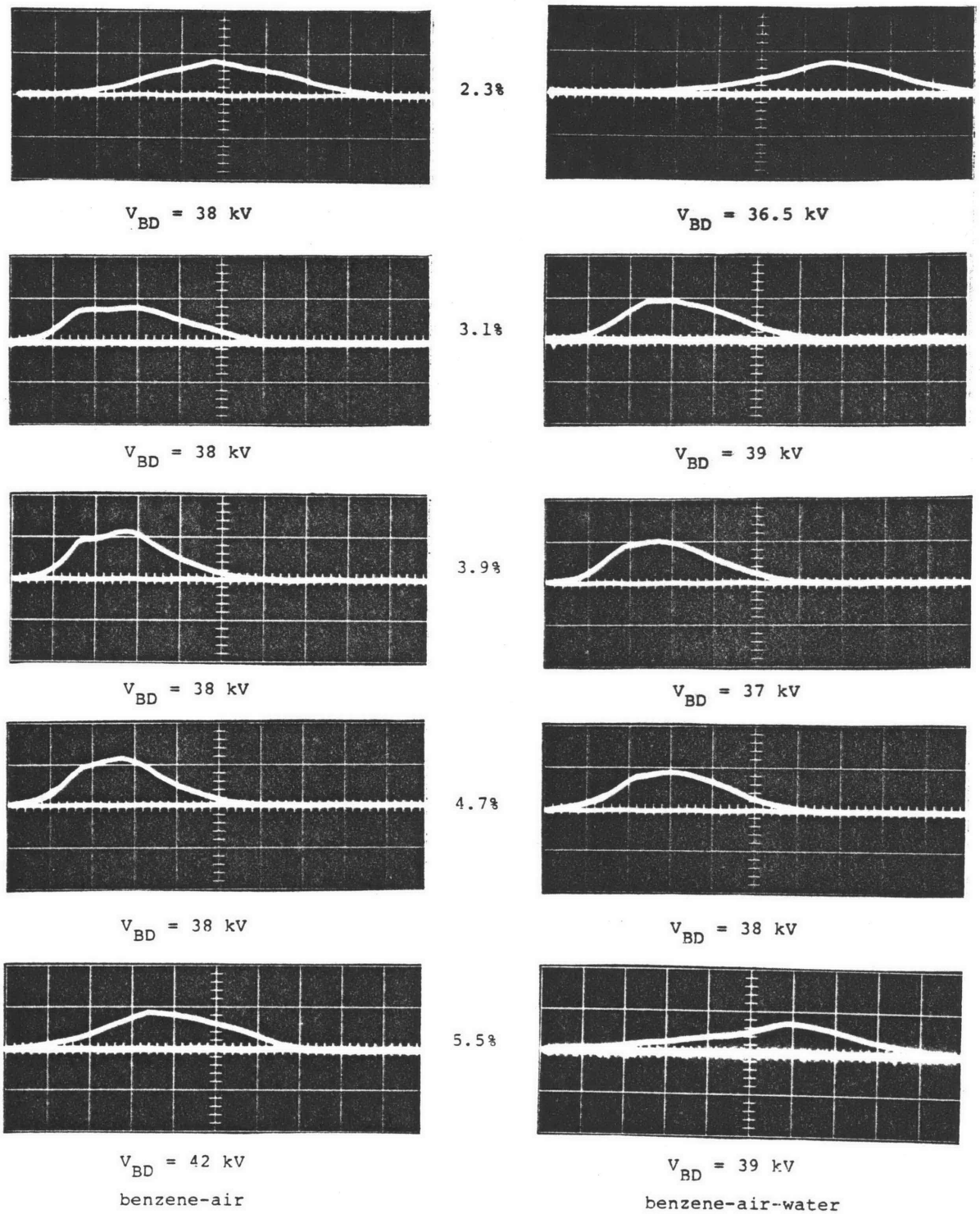

FIGURE 29: Pressure vs time for spark ignited explosive mixtures at 2 cm gap with 1.6 cm radius electrode.
Vertical calibration: 1 box division = 50 psi
Horizontal calibration: 1 box division = 10 milliseconds
Center column: fuel-air composition in % by volume of fuel

introduced also acts as an exhaust valve), hence the creation of the second peak. It will be seen later that this is really the case, when photographs of explosions conducted with wires are portrayed.

By examining Figures 27, 28, and 29 we can see the following:

1. Peak pressure seems to depend on the fuel-air composition. There exists a region, which coincides with the composition where the least amount of energy is required to ignite the mixture, for which the pressure peak has the highest value. This is at 3.95% by volume of fuel. Furthermore, as we move away from this point to either the L.E.L. or the U.E.L., the value of this peak pressure decreases.

2. As was mentioned earlier the velocity of the propagation wave also depends on the concentration of the fuel-air mixture, the highest value occurring again at the point of minimum ignition energy. It is not a coincidence, however, that the highest velocity corresponds to the highest pressure peak. This fact is supported by studies that have been conducted in spherical closed vessels.[20] In effect, a way of calculating velocities at various time intervals in a closed vessel (velocities increase with increasing radius, the explosion taking place at the center of the sphere) is by means of measuring the pressure from a pressure-time record of the explosion.

3. Water acts in a way of slowing down the propagation wave. This can be more easily observed from studying pressure-time records of mixture compositions that are close to either the L.E.L. or the U.E.L. It can be seen that the overall delay in reaching the peak pressure is between 10-25 msec, which in some cases is an

increase of 70% of the time required to reach the pressure peak. As a result of the decrease of the velocity of the flame wave, there is also a decrease in the peak pressure value. This can be readily seen from pictures taken when a smaller test bomb was used. As can be seen from Figure 30 water slows the propagation wave as much as 100%. When more water was added so that a small puddle was created on the bottom plate, the breakdown level dropped by as much as 50%. This will be seen in later photographs.

The breakdown voltage also decreases when water vapor is added to the fuel-air mixture. This decrease is between 2.3% and 17.3%. In a way, water must be acting so as to provide more free electrons travelling towards the anode, hence the lower breakdown voltage for the same gap.

4. By examining the same fuel-air compositions but for different gaps, we see that there is a gap near 0.5 cm, for which the value of the peak pressure is maximum, decreasing either as we shorten or lengthen the electrode distance. The difference may be small, but it exists nevertheless.

5. When the combustion wave approaches the walls of the explosion chamber, it sets up small pressure waves. This happens because the volume of the gas adjacent to the wall is compressed within a small layer and succeedingly expands. The elements closer to the wall travel much faster and it is understandable that towards the end of the process small pressure waves should be set up. These are readily detectable in some pressure-time records of the Figures examined above. In most cases vibrations start before maximum pressure and continue during the cooling period. In order to find

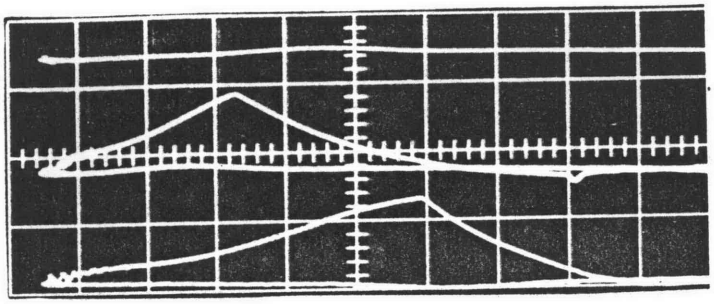

Upper: air only, V_{BD} = 30kV

Middle: 6.6% benzene, V_{BD} = 29kV

Lower: 6.6% benzene and H_2O vapor at saturation, V_{BD} = 29kV

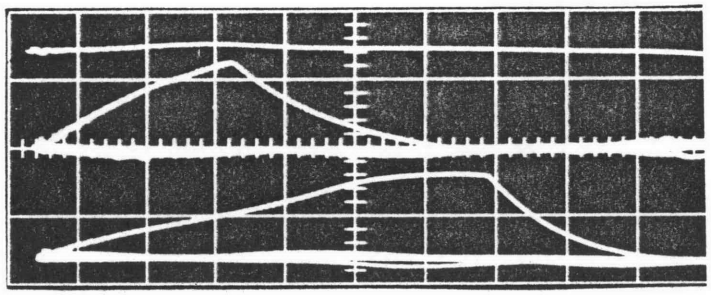

Upper: air only, V_{BD} = 31kV

Middle: 4.4% benzene, V_{BD} = 28kV

Lower: 4.4% benzene and H_2O vapor at saturation, V_{BD} = 26kV

FIGURE 30 Pressure vs time for spark ignited explosive mixtures at 1.5 cm gap with 1.6 cm radius electrode for fuel air compositions as % by volume of fuel.
Vertical calibration: 1 box division = 50 psi
Horizontal calibration: 1 box division = 1 millisecond

the precise limits for which vibrations are observed, more precise tests must be conducted. However, it looks as if the fast-burning mixtures produce bigger vibrations.

6. The level of the peak pressures measured is lower than the one calculated theoretically. The highest values measured were around 75 psi as compared with 145 psi calculated for a constant volume combustion where the equivalence ratio $\Phi = 1$ (see Appendix A). This difference of almost 50% is due to the nature of the model used for the theoretical calculations. The combustion was assumed to be adiabatic while in real life situations there are losses to the walls of the combustion chamber. It is for this reason that differences exist between theoretical calculations and experimental measurements.

In the photographs examined above the reproducibility of the experiments has been checked by repeatedly conducting tests under the sameconditions. This can be seen in many photographs where the pressure-time record of a particular combustion wave is portrayed twice. The results were quite consistent for the most easily ignited mixture but became more variable towards the lower or upper explosive limits.

D. Pressure-time Record; Wire Electrodes

The fact that the pressure would not reach a sharp peak where hemispherical electrodes were used was explained earlier. Figure 31 which represents the pressure-time records of explosions conducted with fuel-air compositions of 3.8% by volume of fuel, helps support what was said earlier. The wires that were used as electrodes were mounted on solid aluminum rods of 1.6 cm diameter hemispherical at one end, and were extending 2.4 cm from the tip of those rods. This in turn allowed the wave to propagate in a spherical manner, especially so when the gap was at its maximum value of 1 cm. It is for this reason that as the gap increases the pressure-time record approaches the ideal one for an explosion. This is readily observed in the above described Figure.

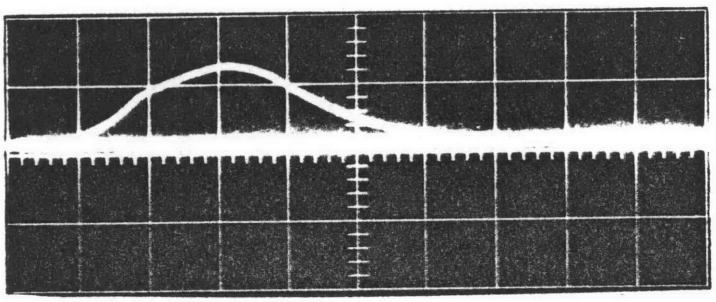

Gap = 0.25 cm
V_{BD} = 3.5kV

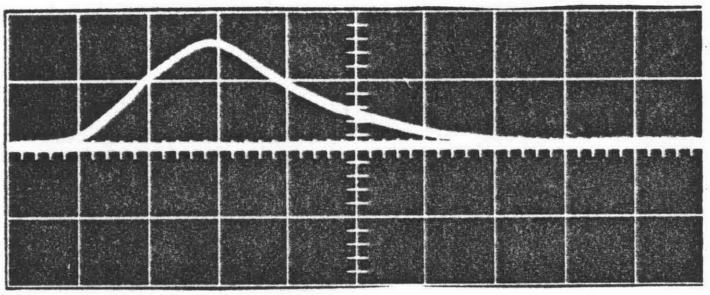

Gap = 0.5 cm
V_{BD} = 6.5kV

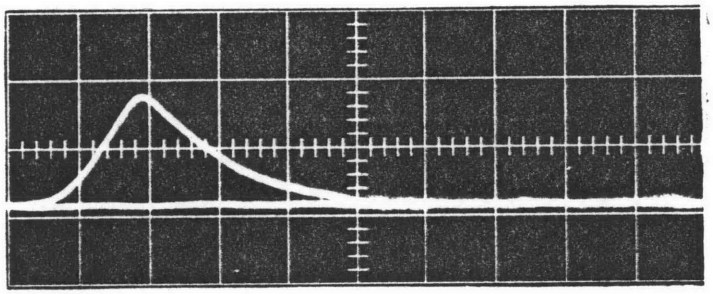

Gap = 1.0 cm
V_{BD} = 11.5kV

FIGURE 31 Pressure vs time for spark ignited explosive mixtures with fuel air compositions of 3.8% by volume of fuel when using steel wire electrodes.
Vertical calibration: 1 box division = 50 psi
Horizontal calibration 1 box division = 10 milliseconds

E. Minimum Ignition Energy

The high voltage capacitive discharge method was used to determine the minimum ignition energies for a particular fuel-air mixture. By employing high voltages and large gaps rather than low voltages and small gaps, the electrodes were separated by an amount greater than the critical flame diameter. To determine minimum ignition energy, a capacitor of known value is charged to a known voltage and discharged through an arc into the mixture. The values of voltage capacitance at the ignition threshold are used to calculate the minimum ignition energy, $1/2\ CV^2$, that had been stored in the circuit prior to the spark discharge. Figure 32 shows a series of pictures characteristic of the procedure for determining the minimum ignition energy. The measurements began with a gap of 0.2 cm. This was then decreased to 0.1 cm where no explosion could be initiated with the circut capacitance of .002934μFd, second picture from top. The capacitance then increased until, by trial and error, the value necessary to just ignite the mixture was found. The last picture shows the explosion after approximately 20 sparks, the haziness of the picture being the result of the sparks occurring before the explosion. The minimum ignition energy for the 0.1 cm gap was thus measured to be 210 mJ.

A thing of interest is that for larger gaps smaller minimum ignition energies were calculated. This happens because the capacitance necessary to ignite the mixture is much much lower, .000017μFd for the 1 cm gap, in contrast with the increase in voltage which changes by a factor of 4. Thus 4.7 J were found sufficient to ignite the mixture at the 1 cm gap. Bigger gaps could result in smaller ignition energies,

but losses due to corona discharges which are substantial, would influence the accuracy of measurements.

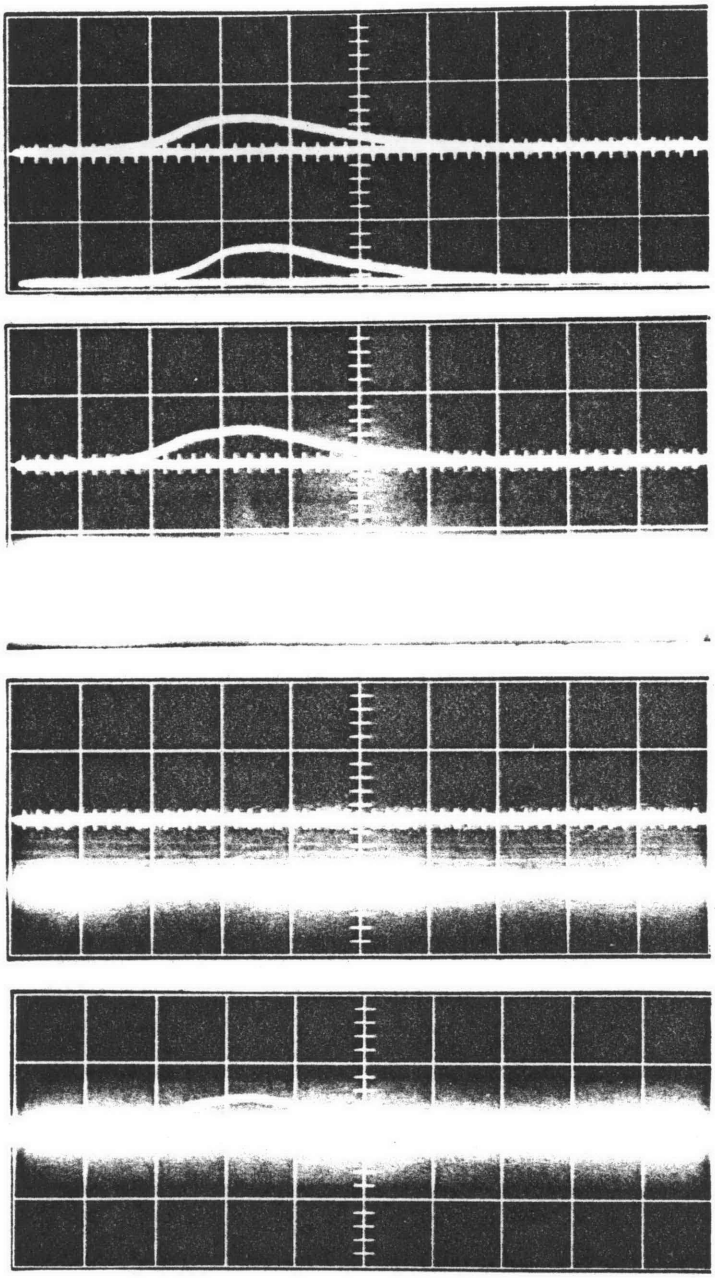

Gap = 0.2 cm
V_{BD} = 7, 6 kV
C = .002934 µFd

Gap = 0.1 cm
No explosion
C = .002934 µFd

Gap = .1 cm
V_{BD} = 5.5kV
C = .052934, .010434 µFd

Gap = 0.1 cm
V_{BD} = 6.5kV
C = .012934 µFd

FIGURE 32 Pressure vs time for benzene air compositions of 4% by volume of fuel with 1.6 cm radius electrode.
Vertical calibration: 1 box division = 50 psi
Horizontal calibration: 1 box division = 10 milliseconds

F. Discharges From Electrostatic Fields

In an effort to examine the possibility of the initiation of an explosion by a static discharge, several tests were conducted. The gap was set at 0.25 cm and an aluminum sphere of 15.24 cm O.D. was charged up. It was found that a total charge accumulation of less than 0.25×10^{-6} coulombs was enough to explode the benzene-air mixture. whose however, while it was possible to perform such explosions when the hemispherical electrodes were used, it was not whenever wires were used instead.

On the other hand an ungrounded person wearing sneakers successfully carried enough charge to initate an explosion when wires were used as electrodes, again for the 0.25 cm gap. This means a charged person would have no difficulty igniting an explosion for more rounded electrodes.

CHAPTER IX

A. Summary

In the previous part, the effects of controlling various parameters on the pressure-time record of an explosion were studied. Figure 33 serves in a way of gathering these effects for a particular gap, namely 1 cm, and a fixed mixture composition of 4.0% by volume of fuel. In the first two pictures the capacitance of the circut was succeedingly lowered from 0.002934 microfarads to 0.000017 microfarads. The next three show the effect of adding water to the mixture up to a point where a puddle of water is formed on the lower electrode. The breakdown voltage drops as more water is added because the field is enhanced by the presence of the high dielectric constant water. Finally, the pressure-time record for using a steel wire is also portrayed.

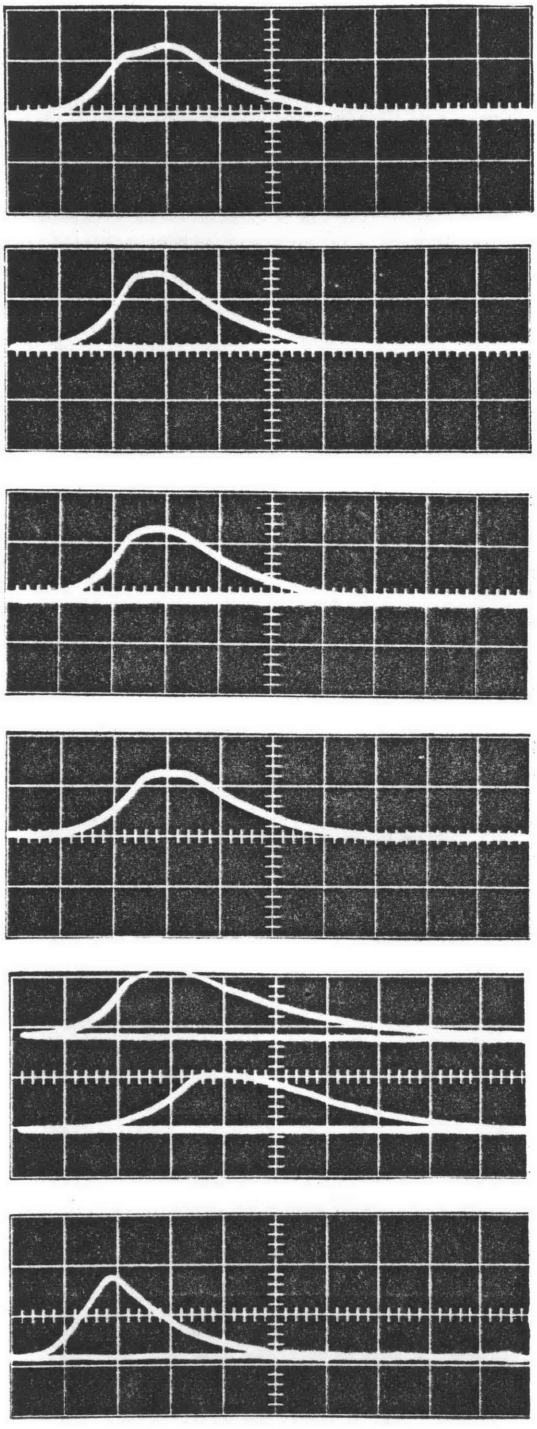

V_{BD} = 24.5 kV
C = .002934 μFd

V_{BD} = 25 kV
C = .000017 μFd

V_{BD} = 23.5 kV
C = .002934 μFd
benzene + 10 μℓ H_2O vapor

V_{BD} = 17 kV
C = .000017 μFd
benzene + 3.5 cc H_2O

V_{BD} = 13,14 kV
C = .002934 μFd
benzene + 5 cc H_2O

V_{BD} = 17 kV
i = 230 μA

FIGURE 33: Pressure vs time for benzene-air compositions of 4% by volume of fuel with 1 cm hemispherical electrode gap, except bottom picture where steel wire electrode was used.

B. Conclusions

The experiments carried out and described in the previous part, help draw the following conclusions:

1. When sufficient energy is discharged, a spark breakdown from either blunt or sharp electrodes will ignite an explosion if the the fuel-air composition lies inside the explosive range.

2. Corona discharge of several hundred microamps with an accompanying bluish glow between the electrodes will not initiate an explosion.

3. The presence of fuel vapor in addition to air, lowers slightly the breakdown voltage. Discharge levels were not dependent on the composition of the fuel-air mixture over the entire explosive range.

4. The presence of water vapor at saturation reduces the velocity of the propagation wave and the voltage necessary for spark breakdown. Furthermore, the addition of water drops lowers the breakdown voltage by as much as a factor of 2.

5. Both the peak pressure and the velocity of the propagation wave attain their maximum values at the fuel-air composition where the least amount of energy is required to ignite the mixture, becoming smaller as we move to either the L.E.L. or the U.E.L.

6. The minimum ignition energy was measured nearly halfway between the explosive limits, increasing as either the L.E.L. or the U.E.L. was approached.

7. Sparks in mixtures outside the explosive limits did not initiate explosions.

8. An isolated statically charged object was sufficient to initiate an explosion.

9. An ungrounded person can carry enough charge to initiate an explosion by a static discharge.

APPENDIX A

MAXIMUM PRESSURE FOR A CONSTANT VOLUME COMBUSTION

Theoretical calculations of the maximum pressure developed in a constant volume combustion chamber with benzene used as the burning fuel are described in this part. The equivalence ratio is defined as $\Phi = \frac{\text{actual fuel air ratio by weight}}{\text{stoichiometric fuel air ratio by weight}}$. The calculations were made for two equivalence ratios namely $\Phi = 0.5$ and $\Phi = 1$. The model used is portrayed in the sketch below with subscripts a for air, f for fuel and p for products.

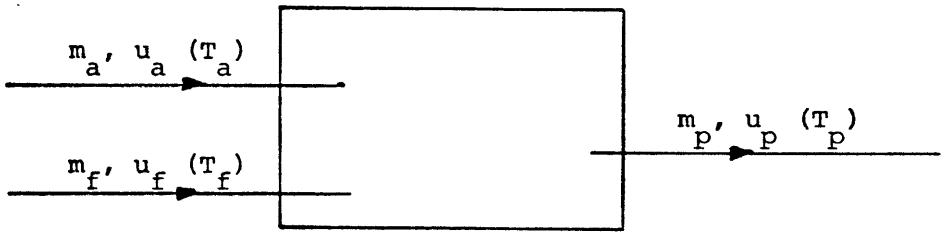

The letters m, u and T are used to denote mass, internal energy and temperature respectively. This constant volume combustion can be described by the equation:

$$m_a[u_a\ (T_a) - u_a\ (T_0)] + m_f\ [u_f\ (T_f) - u_f\ (T_0)] + m_f(\Delta U_L) =$$

$$= m_p[u_p\ (T_p) - u_p\ (T_0)]$$

where ΔU_L denotes the lower heating value of the fuel and the subscript 0 is used to indicate the reference temperature.

If both the air and the fuel are at the reference temperature $T_0 = 77^{\circ}F$ when entering the chamber this relationship becomes

$$m_f\ (\Delta U_L) = m_p[u_p\ (T_p) - u_p\ (T_0)]$$

The temperature of the products was calculated by determining the internal energy of the products of the combustion. For the case with an equivalence ratio $\Phi = 0.5$ the combustion equation is :

$$C_6H_6 + 15(O_2 + 3.76N_2) \rightleftarrows 6CO_2 + 3H_2O + 7.5\ O_2 + 56.4N_2$$

The combustion equation then becomes

$$72.9\ (X - 2708.5) = 1371491 \quad \text{or} \quad X = 21522$$

From combustion tables of products for 200% theoretical air, the corresponding temperature is found to be $2725^{o}R$. By using the perfect gas law the pressure is calculated to be 91 psi. For an equivalence ratio $\Phi = 1$ a similar calculation yields a pressure of 145 psi.

Pressures for fuel rich mixtures cannot be calculated because the quantities of the products are not predictable. It is expected, however, that the maximum pressure will drop for compositions where $\Phi > 1$.

BIBLIOGRAPHY

1. Burnett, A. N. S., "The VLCC Explosions 1, 2, 3", Tanker and Bulk Carrier, 363-364, 410-411, 466-468, December 1970, January 1971, February 1971.

2. "Tank Explosions," Ship and Boat International, 28-29, December 1970.

3. Murphy, F. C., "Tanker Safety; Aim of Explosion Research," World Petroleum, 27-31, July 1971.

4. Hughes, J. F., Bright, A. W., Makin B and Parker, I. F., "A Study of Electrical Discharges in a Changed Water Aerosol," Joul. Phys. D: Appl. Phys., Vol. 6, 966-975, 1973.

5. Schön, G., "Static Electricity and its Ignition Hazards," Electrical Safety Practices, Monograph #13, 102-122, November 1971.

6. D. van der Meer, J. M. van de Weerd, W. Smit and B. Vos: "Electrostatic Charge Generation During Washing of Tanks with Water Sprays," Third Conference of Static Electrification, The Institute of Physics, London, 1971.

7. Lenard, P., "Über du Elektrizität der Wasserfälle," Ann. Phys. Volume 46, 584-636, 1892.

8. Pierce, E. T., "Waterfalls, Bathrooms and - - Perhaps - - Supertanker Explosions," Lightning and Static Electrification Conference, 9-11, December 1970.

9. Pierce, E. T., and Whitson, A. L., "Atmospheric Electricity and the Waterfalls of Yosemite Valley," Journal of Atmospheric Sciences, Volume 22, 314-319, 1965.

10. Matthews, J. B., and Mason, B. J., "Electrification Produced by the Rupture of Large Water Drops in an Electric Field," Quart. J. Royal Meteorol. Society, Volume 90, 275-286, 1964.

11. Levin, Z., and Hobbs, P.V., "Charge Separation Due to Splashing of Water Drops," Conference for Cloud Physics, Fort Collins, 1970.

12. Pierce, E. T., and Whitson, A. L., "Atmospheric Electricity in a Typical American Bathroom," Weather, Volume 21, 449-455, 1966.

13. Cooper, W. J., "Tanker Tank Cleaning Research Program," MSA Research Corporation, March 1974.

14. Reif, R. B., and Hawk, S. A., "Review and Evaluation of the Literature on Electrostatic Generation in Tank Cleaning," Battelle Columbus Laboratories, Final Report, February 1974.

15. Carruthers, J. A. and Wigley, K. J. "The Estimation of Electrostatic Potentials, Fields and Energies in a Rectangular Metal Tank Containing Charged Fuel," Journal of the Institute of Petroleum Volume 48, 1962, pp. 180-195.

16. Vellenga, S. J., "Estimting the Electric Field Inside a Rectangular Tank with Boundaries at Zero Potential," Applied Science Research, Section B, Volume 9, 1961, 35-44.

17. Magison, E. C., "Electrical Instruments in Hazardous Locations," Instrument Society of America, 1962.

18. Lewis, B., and Von Elbe, G., "Combustion Flames and Explosions of Gases," 1961.

19. Bewley, "Two Dimensional Fields in Electrical Engineering," 163.

20. Lewis, B., Pease, R. N., and Taylor, H. S., "Combustion Processes," Volume II, 1956.